nature

https://doi.org/10.1038/d41586-021-03825-4

Accelerated Article Preview

Broadly neutralizing antibodies overcome SARS-CoV-2 Omicron antigenic shift

Received: 12 December 2021

Accepted: 23 December 2021

Accelerated Article Preview
Published online: 23 December 2021

Cite this article as: Cameroni, E. et al. Broadly neutralizing antibodies overcome SARS-CoV-2 Omicron antigenic shift *Nature* https://doi.org/10.1038/d41586-021-03825-4 (2021).

Elisabetta Cameroni, John E. Bowen, Laura E. Rosen, Christian Saliba, Samantha K. Zepeda, Katja Culap, Dora Pinto, Laura A. VanBlargan, Anna De Marco, Julia di Iulio, Fabrizia Zatta, Hannah Kaiser, Julia Noack, Nisar Farhat, Nadine Czudnochowski, Colin Havenar-Daughton, Kaitlin R. Sprouse, Josh R. Dillen, Abigail E. Powell, Alex Chen, Cyrus Maher, Li Yin, David Sun, Leah Soriaga, Jessica Bassi, Chiara Silacci-Fregni, Claes Gustafsson, Nicholas M. Franko, Jenni Logue, Najeeha Talat Iqbal, Ignacio Mazzitelli, Jorge Geffner, Renata Grifantini, Helen Chu, Andrea Gori, Agostino Riva, Olivier Giannini, Alessandro Ceschi, Paolo Ferrari, Pietro E. Cippà, Alessandra Franzetti-Pellanda, Christian Garzoni, Peter J. Halfmann, Yoshihiro Kawaoka, Christy Hebner, Lisa A. Purcell, Luca Piccoli, Matteo Samuele Pizzuto, Alexandra C. Walls, Michael S. Diamond, Amalio Telenti, Herbert W. Virgin, Antonio Lanzavecchia, Gyorgy Snell, David Veesler & Davide Corti

Broadly neutralizing antibodies overcome SARS-CoV-2 Omicron antigenic shift

Elisabetta Cameroni[1*], John E. Bowen[2*], Laura E. Rosen[3*], Christian Saliba[1*], Samantha K. Zepeda[2], Katja Culap[1], Dora Pinto[1], Laura A. VanBlargan[4], Anna De Marco[1], Julia di Iulio[3], Fabrizia Zatta[1], Hannah Kaiser[3], Julia Noack[3], Nisar Farhat[3], Nadine Czudnochowski[3], Colin Havenar-Daughton[3], Kaitlin R. Sprouse[2], Josh R. Dillen[3], Abigail E. Powell[3], Alex Chen[3], Cyrus Maher[3], Li Yin[3], David Sun[3], Leah Soriaga[3], Jessica Bassi[1], Chiara Silacci-Fregni[1], Claes Gustafsson[5], Nicholas M. Franko[6], Jenni Logue[6], Najeeha Talat Iqbal[7], Ignacio Mazzitelli[8], Jorge Geffner[8], Renata Grifantini[9], Helen Chu[6], Andrea Gori[10], Agostino Riva[11], Olivier Giannini[12,13], Alessandro Ceschi[12,14,15,16], Paolo Ferrari[12,17,18], Pietro E. Cippà[13,17,19], Alessandra Franzetti-Pellanda[20], Christian Garzoni[21], Peter J. Halfmann[22], Yoshihiro Kawaoka[22,23,24], Christy Hebner[3], Lisa A. Purcell[3], Luca Piccoli[1], Matteo Samuele Pizzuto[1], Alexandra C. Walls[2,25], Michael S. Diamond[4,26,27], Amalio Telenti[3], Herbert W. Virgin[3,26,28,29], Antonio Lanzavecchia[1,9,29], Gyorgy Snell[3,29], David Veesler[2,25,29], Davide Corti[1,29]

[1]Humabs Biomed SA, a subsidiary of Vir Biotechnology, 6500 Bellinzona, Switzerland
[2]Department of Biochemistry, University of Washington, Seattle, WA 98195, USA
[3]Vir Biotechnology, San Francisco, California 94158, USA
[4]Department of Medicine, Washington University of School of Medicine, St. Louis, MO, USA
[5]ATUM, Newark, California 94560, USA
[6]Division of Allergy and Infectious Diseases, University of Washington, Seattle, WA 98195, USA.
[7]Department of Paediatrics and Child Health, Aga Khan University, Karachi, 74800, Pakistan
[8]Instituto de Investigaciones Biomédicas en Retrovirus y SIDA (INBIRS), Facultad de Medicina, Buenos Aires C1121ABG, Argentina
[9]National Institute of Molecular Genetics, Milano, Italy
[10]Infectious Disease Unit, Fondazione IRCCS Ca' Granda, Ospedale Maggiore Policlinico, Milan, Italy
[11]Department of Biomedical and Clinical Sciences 'L.Sacco' (DIBIC), Università di Milano, Milan, Italy
[12]Faculty of Biomedical Sciences, Università della Svizzera italiana, Lugano, Switzerland
[13]Department of Medicine, Ente Ospedaliero Cantonale, Bellinzona, Switzerland
[14]Clinical Trial Unit, Ente Ospedaliero Cantonale, Lugano, Switzerland
[15]Division of Clinical Pharmacology and Toxicology, Institute of Pharmacological Science of Southern Switzerland, Ente Ospedaliero Cantonale, Lugano, Switzerland
[16]Department of Clinical Pharmacology and Toxicology, University Hospital Zurich, Zurich, Switzerland
[17]Division of Nephrology, Ente Ospedaliero Cantonale, Lugano, Switzerland
[18]Clinical School, University of New South Wales, Sydney, Australia
[19]Faculty of Medicine, University of Zurich, 8057 Zurich, Switzerland
[20]Clinical Research Unit, Clinica Luganese Moncucco, 6900 Lugano, Switzerland
[21]Clinic of Internal Medicine and Infectious Diseases, Clinica Luganese Moncucco, 6900 Lugano, Switzerland.
[22]Influenza Research Institute, Department of Pathobiological Sciences, School of Veterinary Medicine, University of Wisconsin-Madison, Madison, WI, USA
[23]Division of Virology, Department of Microbiology and Immunology, Institute of Medical Science, University of Tokyo, 108-8639 Tokyo, Japan
[24]The Research Center for Global Viral Diseases, National Center for Global Health and Medicine Research Institute, Tokyo 162-8655, Japan
[25]Howard Hughes Medical Institute, Seattle, WA 98195, USA.
[26]Department of Pathology and Immunology, Washington University School of Medicine, St. Louis, MO, USA
[27]Department of Molecular Microbiology, Washington University School of Medicine, St. Louis, MO, USA
[28]Department of Internal Medicine, UT Southwestern Medical Center, Dallas TX 75390
[29]These authors contributed equally: Herbert W. Virgin, Antonio Lanzavecchia, David Veesler, Gyorgy Snell and Davide Corti

[*]These authors contributed equally
Correspondence: dcorti@vir.bio, dveesler@uw.edu, gsnell@vir.bio

Keywords: SARS-CoV-2; COVID-19; antibody, vaccine, neutralizing antibodies; immune evasion

SUMMARY:

The recently emerged SARS-CoV-2 Omicron variant encodes 37 amino acid substitutions in the spike (S) protein, 15 of which are in the receptor-binding domain (RBD), thereby raising concerns about the effectiveness of available vaccines and antibody therapeutics. Here, we show that the Omicron RBD binds to human ACE2 with enhanced affinity, relative to the Wuhan-Hu-1 RBD, and binds to mouse ACE2. Marked reductions of plasma neutralizing activity were observed against Omicron compared to the ancestral pseudovirus for convalescent and vaccinated individuals, but this loss was less pronounced after a third vaccine dose. Most receptor-binding motif (RBM)-directed monoclonal antibodies (mAbs) lost in vitro neutralizing activity against Omicron, with only 3 out of 29 mAbs retaining unaltered potency, including the ACE2-mimicking S2K146 mAb[1]. Furthermore, a fraction of broadly neutralizing sarbecovirus mAbs neutralized Omicron through recognition of antigenic sites outside the RBM, including sotrovimab[2], S2X259[3] and S2H97[4]. The magnitude of Omicron-mediated immune evasion marks a major SARS-CoV-2 antigenic shift. Broadly neutralizing mAbs recognizing RBD epitopes conserved among SARS-CoV-2 variants and other sarbecoviruses may prove key to controlling the ongoing pandemic and future zoonotic spillovers.

INTRODUCTION

The evolution of RNA viruses can result in immune escape and modulation of binding to host receptors through accumulation of mutations[5]. Previously emerged SARS-CoV-2 variants of concern (VOC) have developed resistance to neutralizing antibodies, including some clinical antibodies used as therapeutics[6-8]. The B.1.351 (Beta) VOC is endowed with the greatest magnitude of immune evasion from serum neutralizing antibodies[6,7], whereas B.1.617.2 (Delta) quickly outcompeted all other circulating isolates through acquisition of mutations that enhanced transmission and pathogenicity[9-11] and eroded the neutralizing activity of antibody responses[9].

The Omicron (B.1.1.529) variant was first detected in November 2021, immediately declared by the WHO as a VOC and quickly rose in frequency worldwide. The Omicron variant is substantially mutated compared to any previously described SARS-CoV-2 isolates, including 37 S residue substitutions in the predominant haplotype (**Fig. 1a** and **Extended Data Fig. 1-4**). Fifteen of the Omicron mutations are clustered in the RBD, which is the main target of neutralizing antibodies after infection or vaccination[12,13], suggesting that Omicron might escape infection- and vaccine-elicited Abs and therapeutic mAbs. Nine of these mutations map to the receptor-binding motif (RBM) which is the RBD subdomain directly interacting with the host receptor, ACE2[14].

Preliminary reports indicated that the neutralizing activity of plasma from Pfizer-BioNTech BNT162b2 vaccinated individuals is reduced against SARS-CoV-2 Omicron[15,16], documenting a substantial, albeit not complete, escape from mRNA vaccine-elicited neutralizing antibodies. Another report also shows that vaccine effectiveness against symptomatic disease induced by the Omicron variant is significantly lower than for the Delta variant[17]. The potential for booster doses to ameliorate this decline in neutralization is being explored. In addition, the neutralizing activity of several therapeutic mAbs appears decreased or abolished against SARS-CoV-2 Omicron[16,18].

To understand the consequences of the unprecedented number of mutations found in Omicron S, we employed a pseudovirus assay to study receptor usage and neutralization mediated by monoclonal and polyclonal antibodies as well as surface plasmon resonance to measure binding of the RBD to human and mouse ACE2 receptors.

RESULTS

The Omicron RBD binds with increased affinity to human ACE2 and gains binding to mouse ACE2

Twenty-three out of the 37 Omicron S amino acid mutations have been individually observed previously in SARS-CoV-2 variants of interest (VOI), VOC, or other sarbecoviruses, whereas the remaining 14 substitutions have not been described before (**Extended Data Fig. 5a**). Analysis of the GISAID database indicates that there are rarely more than 10-15 Omicron S mutations present in a given non-Omicron haplotype or Pango lineage (**Extended Data Fig. 5b-d)**. While we have not formally assessed the possibility of recombination events, persistent replication in immunocompromised individuals or inter-species ping-pong transmission[5] are possible scenarios for the rapid accumulation of mutations that could have been selected based on viral fitness and immune evasion.

Several of the Omicron RBD mutations are found at positions that are key contact sites with human ACE2, such as K417N, Q493K and G496S[19]. Except for N501Y, which increases ACE2 binding affinity by 6-fold[20,21], all other substitutions were shown by deep mutational scanning (DMS) to either reduce binding or to have no impact on human ACE2 affinity when present individually[22], resulting in an overall predicted decrease of binding affinity (**Supplementary Table 1**). However, we found that the Omicron RBD has a 2.4-fold increased binding affinity to human ACE2 (**Fig. 1b, c** and **Extended Data Figure 6a**), suggesting epistasis of the full constellation of RBD mutations. It remains to be determined whether and how the S mutations in Omicron may influence the dynamics of RBD opening, which may also impact RBD engagement with ACE2.

The presence of the N501Y mutation has previously been described to enable some SARS-CoV-2 VOC to infect mice[23]. Since Omicron carries the N501Y mutation, along with 14 other RBD mutations, we investigated whether the Omicron RBD binds mouse ACE2 using surface plasmon resonance (SPR) (**Fig. 1b** and **Extended Data Fig. 6**). The Omicron RBD binds mouse ACE2 with a 1:1 binding affinity of 470 nM (**Fig. 1b**), whereas weak binding of the Beta RBD and very weak binding of the Alpha RBD to mouse ACE2 was observed (**Fig. 1b** and **Extended Data Fig. 6b**), consistent with previous reports[23,24]. Conversely, our assay did not detect any binding of the Wuhan-Hu-1, Delta, or K417N RBDs to mouse ACE2. The enhanced binding of

the Omicron RBD to mouse ACE2 is likely explained by the Q493R substitution which is similar to the Q493K mutation isolated upon mouse-adaptation of SARS-CoV-2[19]. Our binding data correlate with our observation of Omicron S-mediated but not Wuhan-Hu-1/G614 S-mediated entry of VSV pseudoviruses into mouse ACE2-expressing cells **(Fig 1d)**, as recently reported[25]. Collectively, these findings highlight the plasticity of the SARS-CoV-2 RBM, which in the case of the Omicron VOC acquired enhanced binding to human and mouse ACE2 orthologues, relative to other SARS-CoV-2 isolates. The influence of these findings on viral load and replication kinetics in humans and animal models remains to be evaluated due to the interplay of additional factors besides receptor binding. Preliminary data, suggest that Omicron appears attenuated in some laboratory mouse strains (M.S.D, personal communication) and that replicates less efficiently in human lung tissue as compared to Delta[26].

Extent of Omicron escape from polyclonal plasma neutralizing antibodies

To investigate the magnitude of immune evasion mediated by the 37 mutations present in Omicron S, we used Wuhan-Hu-1 S and Omicron S VSV pseudoviruses and compared plasma neutralizing activity in different cohorts of convalescent patients or individuals vaccinated with six major COVID-19 vaccines (mRNA-1273, BNT162b2, AZD1222, Ad26.COV2.S, Sputnik V and BBIBP-CorV) (**Fig. 2**, **Supplementary Fig. 1-3** and **Extended Data Table 1**).

Convalescent patients and individuals vaccinated with Ad26.COV2.S (single dose), Sputnik V or BBIBP-CorV had no detectable neutralizing activity against Omicron except for one Ad26.COV2.S and three BBIBP-CorV vaccine recipients (**Fig. 2a**). Individuals immunized with mRNA-1273, BNT162b2, and AZD1222 had more potent neutralizing activity against Wuhan-Hu-1 and retained detectable neutralization against Omicron with a decrease of 39-, 37- and 21-fold, respectively (**Fig. 2a**). The dampening of neutralizing activity against Omicron was comparable to that observed against SARS-CoV, a virus that differs from Wuhan-Hu-1 by 52 residues in the RBD. Reductions of neutralization potency were less pronounced in vaccinated individuals who had been previously infected (5-fold) (**Fig. 2b**) and in dialysis patients (4-fold, **Fig. 2c**) who were boosted with a third mRNA vaccine dose. In the same cohort of dialysis patients, antibodies neutralizing the vaccine-matched Wuhan-Hu-1 strain were found to be low (less than 1/100) or undetectable in 44% of patients after the second mRNA vaccine dose[27].

Collectively, these findings demonstrate a substantial and unprecedented reduction in plasma neutralizing activity against Omicron as compared to the ancestral virus, which in several cases likely falls below the protective threshold[28]. Our data further indicate that multiple exposures to the ancestral virus through infection or vaccination results in the production of antibodies that can neutralize divergent viruses, such as Omicron or even SARS-CoV, as a consequence of affinity maturation or epitope masking by immune-dominant RBM antibodies[28-30].

Broadly neutralizing sarbecovirus antibodies inhibit SARS-CoV-2 Omicron

Neutralizing mAbs with demonstrated in vivo efficacy in prevention or treatment of SARS-CoV-2[31-37] can be divided into two groups based on whether they do or do not block S binding to ACE2. Of the eight currently authorized or approved mAbs, seven (LY-CoV555, LY-CoV016, REGN10933, REGN10933, COV2-2130, COV2-2196 and CT-P59; all synthesized based on publicly available sequences) block binding of S to ACE2 and are often used as two-mAb cocktails[8]. They bind to epitopes overlapping with the RBM (**Fig. 3a**) which is structurally and evolutionary plastic[38], as illustrated by the accumulation of mutations throughout the pandemic and the genetic diversity of this subdomain among ACE2-utilizing sarbecoviruses[39]. Combining two such ACE2 blocking mAbs can provide greater resistance to variant viruses that carry RBM mutations[31]. The second class of mAbs, represented by sotrovimab, do not block ACE2 binding but neutralize SARS-CoV-2 by targeting non-RBM epitopes shared across many sarbecoviruses, including SARS-CoV[4,40].

We compared the *in vitro* neutralizing activity of these therapeutic mAbs side-by-side against Wuhan-Hu-1 S and Omicron S using VSV pseudoviruses (**Fig. 3**). Although sotrovimab had 3-fold reduced potency against Omicron and Omicron-R346K variant VSV pseudoviruses, all other (RBM-specific) mAbs completely lost their neutralizing activity, with the exception of the combination of COV2-2130 and COV2-2196 for which we determined a ~100-fold reduced potency (**Fig. 3b-c**). Moreover, sotrovimab exhibited a less than 2-fold reduction in neutralizing activity against authentic Omicron SARS-CoV-2 as compared to the WA1/2020 D614G virus (**Fig. 3c** and **Extended Data Fig. 7**), consistent with recent reports on S309, the parent of sotrovimab[41,42]. The 3-fold and less than 2-fold decrease in the neutralizing activity of sotrovimab against pseudoviruses and authentic virus, respectively, is within the currently defined threshold of "no change" as defined by FDA (FDA fact sheet for sotrovimab denotes no change: <5-fold

196 reduction in susceptibility[43]). Overall, our findings agree with two preliminary reports[16,18] and,
197 together with serological data, support that the Omicron VOC has undergone antigenic shift.
198 We next tested a larger panel of 36 neutralizing NTD- or RBD-specific mAbs for which
199 the epitopes have been characterized structurally or assigned to a given antigenic site through
200 competition studies[3,4,9,12,44,45] (**Fig. 4a, Extended Data Table 2** and **Extended Data Fig. 8**). The
201 four NTD-specific antibodies completely lost activity against Omicron, consistent with the
202 presence of mutations and deletions in the NTD antigenic supersite[21,46]. Three out of the 22 mAbs
203 targeting the RBD antigenic site I (RBM) retained potent neutralizing activity against Omicron,
204 including S2K146, which binds the RBD of SARS-CoV-2, SARS-CoV and other sarbecoviruses
205 through ACE2 molecular mimicry[1]. Of the nine mAbs specific for the conserved RBD site II[4],
206 only S2X259[3] retained activity against Omicron, whereas neutralization was decreased by more
207 than 10-fold or abolished for the remaining mAbs. Finally, the S2H97 mAb retained neutralizing
208 activity against Omicron through recognition of the highly conserved cryptic site V[4]. The panel
209 of 44 mAbs tested in this study includes members of each of the four classes of neutralizing mAbs,
210 defined by their cognate RBD binding sites (site I, II, IV and V)[12]. Our findings show that
211 member(s) of each of the four classes can retain Omicron neutralization: S2K146, S2X324 and
212 S2N28 targeting site I, S2X259 targeting site II, sotrovimab targeting site IV, and S2H97 targeting
213 site V (**Fig. 4b**). Several of these mAbs cross-react with and neutralize sarbecoviruses beyond the
214 SARS-CoV-2 clade 1b[1,3,4], indicating that targeting of conserved epitopes can lead to
215 neutralization breadth and resilience to antigenic shift associated with viral evolution.
216
217 **Discussion**
218 The remarkable number of substitutions present in Omicron S marks a dramatic shift in
219 antigenicity and is associated with immune evasion of unprecedented magnitude for SARS-CoV-
220 2. While antigenic shift of the influenza virus is defined as genetic reassortment of the RNA
221 genome segments, the mechanism for the abrupt appearance of a large number of mutations in
222 SARS-CoV-2 Omicron S remains to be determined. Although recombination events are a hallmark
223 of coronaviruses[47], we and others[48] propose that the Omicron shift may result from extensive viral
224 replication in immunodeficient hosts[47,49], although we cannot rule out the possibility of a
225 contribution of inter-species ping-pong transmission[5] between humans and rodents, as previously
226 described for minks[50].

Consistent with the variable decrease in plasma neutralizing antibody titers, we found that only six out of a panel of 44 neutralizing mAbs retained potent neutralizing activity against Omicron. The mAbs retaining neutralization recognize RBD antigenic sites that are conserved in Omicron and other sarbecoviruses. Notably, three of these mAbs bind to the RBM, including one which is a molecular mimic of the ACE2 receptor (S2K146)[1]. Collectively, these data may guide future efforts to develop SARS-CoV-2 vaccines and therapies to counteract antigenic shift and future sarbecovirus zoonotic spillovers.

Acknowledgements

We thank Hideki Tani (University of Toyama) for providing the reagents necessary for preparing VSV pseudotyped viruses. This study was supported by the National Institute of Allergy and Infectious Diseases (DP1AI158186 and HHSN272201700059C to D.V.), a Pew Biomedical Scholars Award (D.V.), an Investigators in the Pathogenesis of Infectious Disease Awards from the Burroughs Wellcome Fund (D.V.), Fast Grants (D.V.), the National Institute of General Medical Sciences (5T32GM008268-32 to SKZ). D.V. is an Investigator of the Howard Hughes Medical Institute. OG is funded by the Swiss Kidney Foundation. This work was supported, in part, by the National Institutes of Allergy and Infectious Diseases Center for Research on Influenza Pathogenesis (HHSN272201400008C), Center for Research on Influenza Pathogenesis and Transmission (CRIPT) (75N93021C00014), and the Japan Program for Infectious Diseases Research and Infrastructure (JP21wm0125002) from the Japan Agency for Medical Research and Development (AMED).

Author contributions

Conceived research and designed study: D.C., G.S., M.S.P., L.P., D.V. Designed experiments: D.C., D.P., E.C., L.E.R., G.S., M.S.P., L.P., J.E.B., S.K.Z., A.C.W., D.V. Designed and performed mutagenesis for S mutant expression plasmids: E.C. and K.C. Produced pseudoviruses: C.S., D.P., H.K., J.N., N.F., K.R.S. and S.K.Z. Carried out pseudovirus entry or neutralization assays: C.S., J.E.B., S.K.Z., D.P., F.Z., J.B., C.S-F. and A.D.M. C.S., K.C. and E.C. expressed antibodies. Isolation and propagation of SARS-CoV-2 Omicron live virus: L.A.V., P.J.H., Y.K. Performed authentic virus neutralization assays: L.A.V. Supervised the research on authentic virus neutralization assays: M.S.D. L.E.R. performed binding assays. Cl.G., S.K.Z., A.C.W., N.C., A.E.P. and J.R.D. synthesized expression plasmid, expressed and purified ACE2 and RBD proteins. Production and quality control of mAbs: C.S., A.C. Bioinformatic and epidemiology analyses: J.diI., C.M., L.Y., D.S., L.S. Interpreted Data: C.S., D.P., L.P., L.E.R., M.S.P., A.D.M. Data analysis: E.C., C.S., F.Z., A.D.M., K.C., D.P., J.E.B., L.E.R., S.K.Z., A.C.W., D.V., A.T., G.S., D.C. A.R., O.G., Ch.G., A.C., P.F., A.F.P., H.C., N.M.F., J.L., N.T.I., I.M., J.G., R.G., A.G, P.C. and C.H.D. contributed to donors recruitment and plasma samples collection. D.C., A.L., H.W.V., G.S., A.T., L.A.P., D.V., wrote the manuscript with input from all authors.

Competing interests

E.C., K.C., C.S., D.P., F.Z., A.D.M., A.L., L.P., M.S.P., D.C., H.K., J.N., N.F., J.diI., L.E.R., N.C., C.H.D., K.R.S., J.R.D., A.E.P., A.C., C.M., L.Y., D.S., L.S., L.A.P. , C.H., A.T., H.W.V. and G.S. are employees of Vir Biotechnology Inc. and may hold shares in Vir Biotechnology Inc. L.A.P. is a former employee and shareholder in Regeneron Pharmaceuticals. Regeneron provided no funding for this work. H.W.V. is a founder and hold shares in PierianDx and Casma Therapeutics. Neither company provided resources. The Veesler laboratory has received a sponsored research agreement from Vir Biotechnology Inc. HYC reported consulting with Ellume, Pfizer, The Bill and Melinda Gates Foundation, Glaxo Smith Kline, and Merck. She has received research funding from Emergent Ventures, Gates Ventures, Sanofi Pasteur, The Bill and Melinda Gates Foundation, and support and reagents from Ellume and Cepheid outside of the submitted work. M.S.D. is a consultant for Inbios, Vir Biotechnology, Senda Biosciences, and Carnival Corporation, and on the Scientific Advisory Boards of Moderna and Immunome. The Diamond laboratory has received funding support in sponsored research agreements from Moderna, Vir Biotechnology, and Emergent BioSolutions. The remaining authors declare that the research was conducted in the

absence of any commercial or financial relationships that could be construed as a potential conflict of interest.

Fig. 1

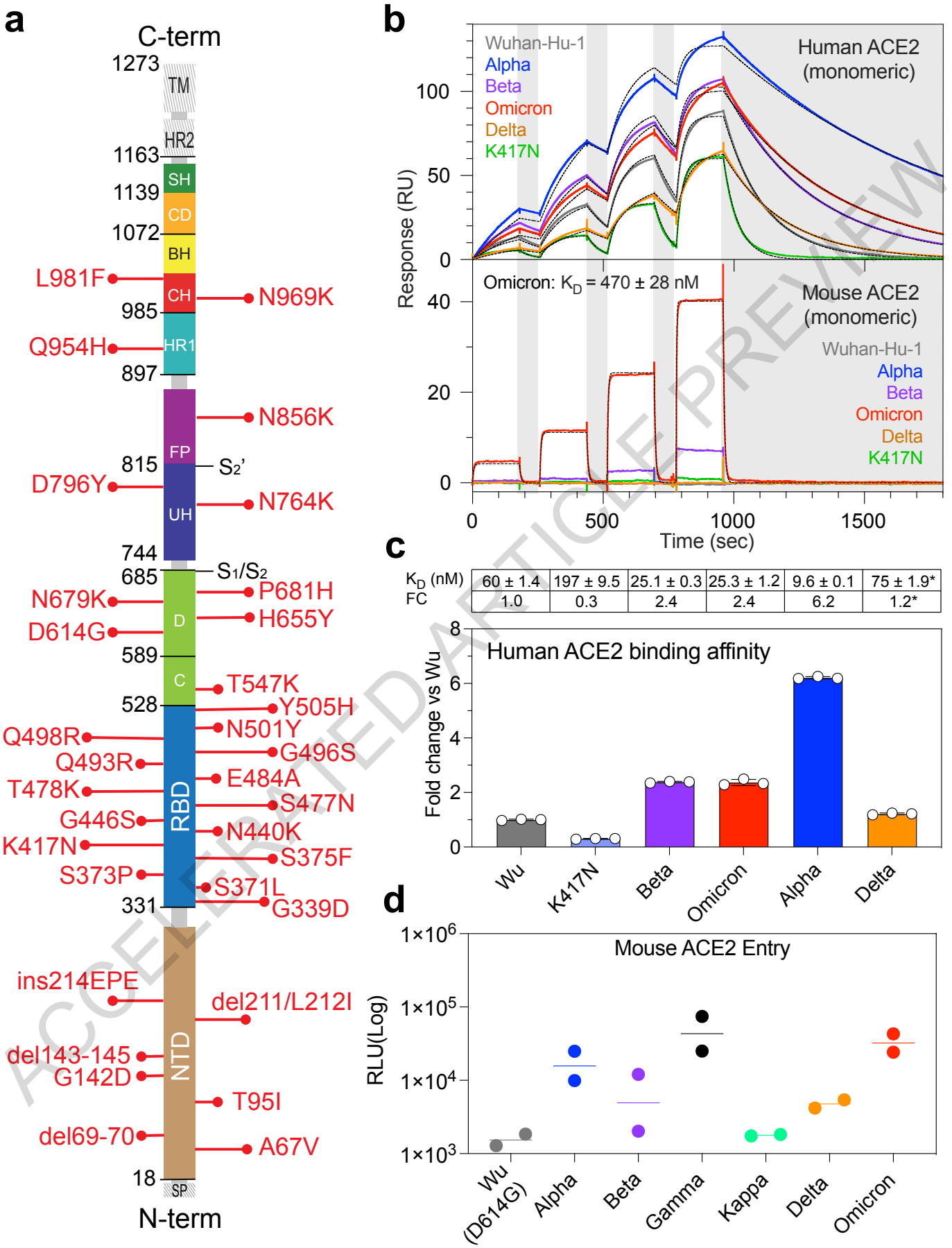

FIGURE LEGENDS.

Fig. 1. Omicron RBD shows increased binding to human ACE2 and gains binding to murine ACE2. **a,** Omicron mutations are shown in a primary structure of SARS-CoV-2 S with domains and cleavage sites highlighted. **b**, Single-cycle kinetics SPR analysis of ACE2 binding to six RBD variants. ACE2 is injected successively at 11, 33, 100, and 300 nM (human) or 33, 100, 300, and 900 nM (mouse). Black curves show fits to a 1:1 binding model. White and gray stripes indicate association and dissociation phases, respectively. **c,** Quantification of human ACE2 binding data. Reporting average ± standard deviation of three replicates. Asterisks indicate that Delta was measured in a separate experiment with a different chip surface and capture tag; Delta fold-change is calculated relative to affinity of Wuhan-Hu-1 measured in parallel (91 ± 1.6 nM). **d,** Entry of Wu-Hu-1, Alpha, Beta, Delta, Gamma, Kappa and Omicron VSV pseudoviruses into mouse ACE2 expressing HEK293T cells. Shown are 2 biological replicates (technical triplicates). Lines, geometric mean.

Fig. 2

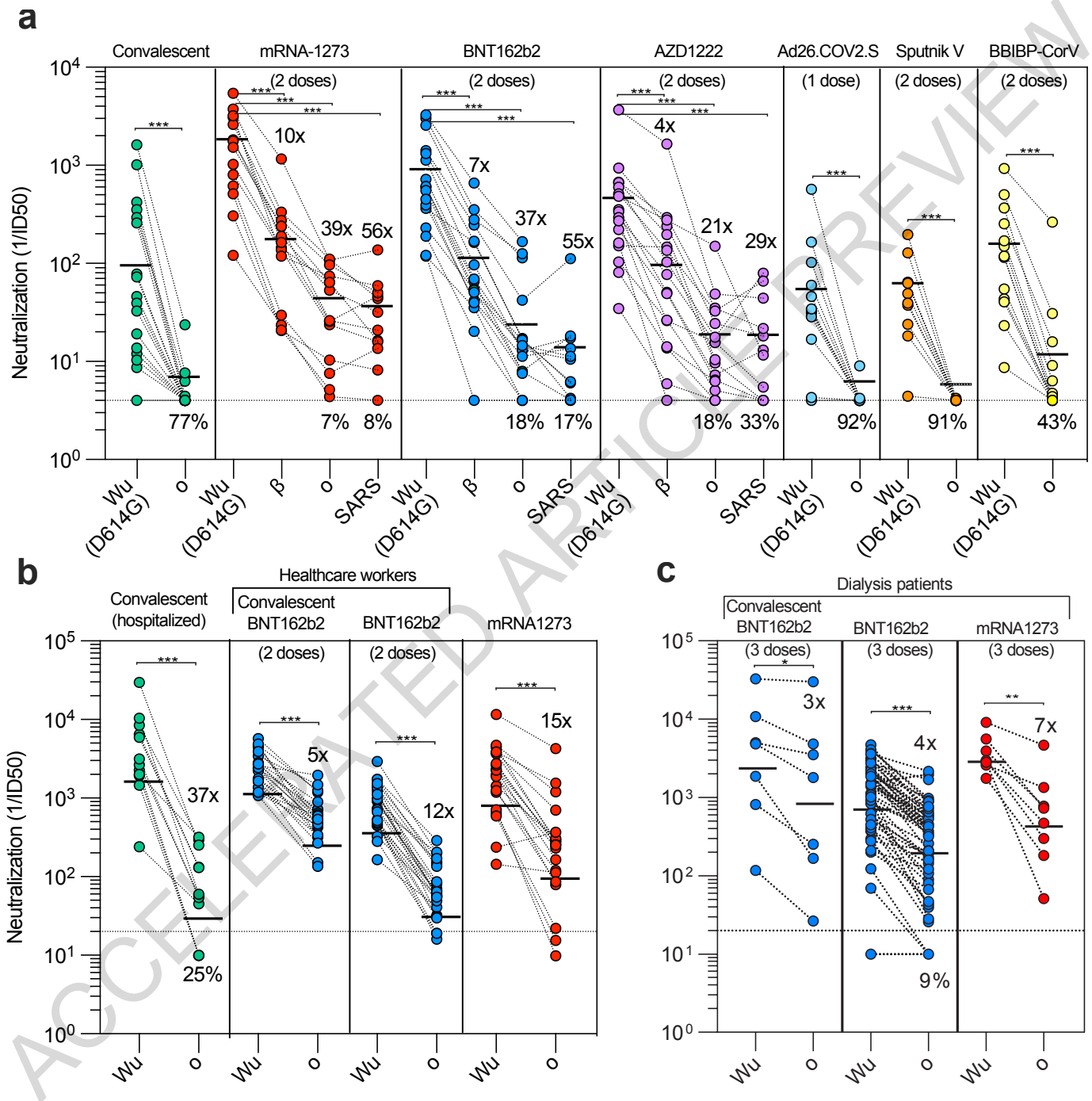

Fig. 2. Neutralization of Omicron SARS-CoV-2 VSV pseudovirus by plasma from COVID-19 convalescent and vaccinated individuals. Plasma neutralizing activity in COVID-19 convalescent or vaccinated individuals (mRNA-1273, BNT162b2, AZD1222, Ad26.COV2.S (single dose), Sputnik V and BBIBP-CorV). **a,** Pairwise neutralizing antibody titers (ID50) against Wuhan-Hu-1 (D614G), Beta, and Omicron VOC, and SARS-CoV. Vero E6-TMPRSS2 used as target cells. Data are geometric mean of n = 3 biologically independent experiments. **b**, Pairwise neutralizing antibody titers of plasma (ID50) against Wuhan-Hu-1 and Omicron VOC. Data are geometric mean of n = 2 biologically independent experiments. **c**, Plasma neutralizing activity in dialysis patients who received 3 doses of either BNT162b2 or mRNA-1273 mRNA vaccines. Pairwise neutralizing antibody titers of plasma (ID50) against Wuhan-Hu-1 and Omicron. One representative experiment out of two is shown. Vero E6 used as target cells in **b** and **c**. Line, geometric mean of 1/ID50 titers. Shown is the percentage of samples that lost detectable neutralization against Omicron or SARS-CoV. Shown cumulative titer loss not accounting samples with 1/ID50 below the limit of detection. HCW, healthcare workers; Wu, Wuhan-Hu-1; o, Omicron VOC, b, Beta VOC. Enrolled donors' demographics provided in **Extended Data Table 1**. Statistical significance is set as $P<0.05$ and P-values are indicated with asterisks (*=0.033; **=0.002; ***<0.001), using a paired two-sided t test (Wilcoxon rank test).

Fig. 3

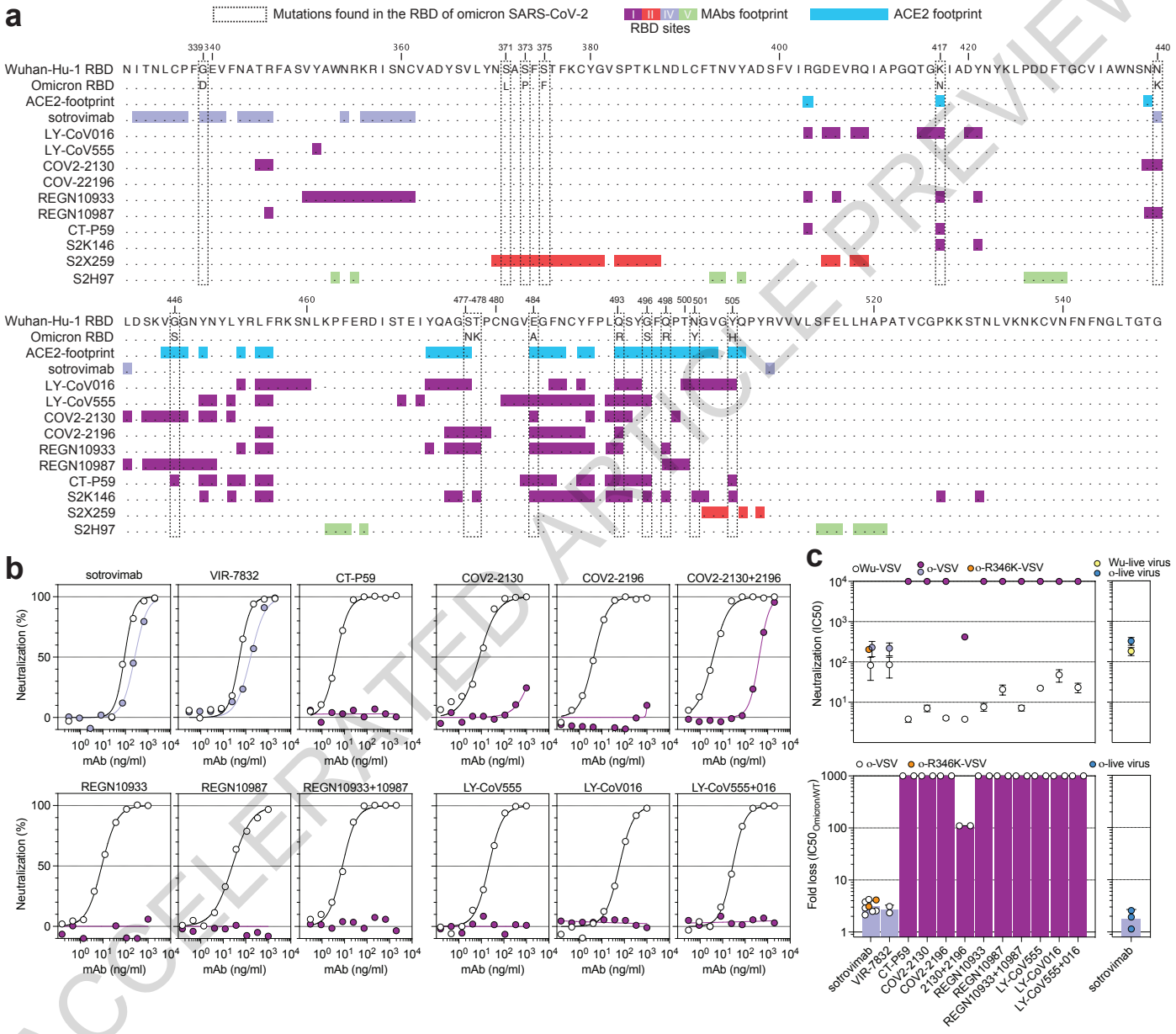

Fig. 3. Neutralization of Omicron SARS-CoV-2 VSV pseudovirus by clinical-stage mAbs. a, RBD sequence of SARS-CoV-2 Wuhan-Hu-1 with highlighted footprints of ACE2 (light blue) and mAbs (colored according to the RBD antigenic site recognized). Omicron RBD is also shown, and amino acid substitutions are boxed. **b,** Neutralization of SARS-CoV-2 VSV pseudoviruses displaying Wuhan-Hu-1 (white) or Omicron (colored as in **Fig. 4b**) S proteins by clinical-stage mAbs. Data are representative of one independent experiment out of two. Shown is the mean of 2 technical replicates. **c,** Geometric mean IC50 values for Omicron (colored as in Fig. 4b) and Wuhan-Hu-1 (white) (top panel), and geometric mean fold change (bottom panel). Vero E6 used as target cells. Shown in blue (right) is neutralization of authentic virus by sotrovimab (WA1/2020 versus hCoV-19/USA/WI-WSLH-221686/2021). Non-neutralizing IC50 titers and fold change were set to 10^4 and 10^3, respectively. Orange dots for sotrovimab indicate neutralization of Omicron VSV pseudovirus carrying R346K. Data are representative of n = 2 biologically independent experiments for most mAbs, for sotrovimab against Omicron VSV n=6 and for Omicron authentic virus n=3.

Fig. 4

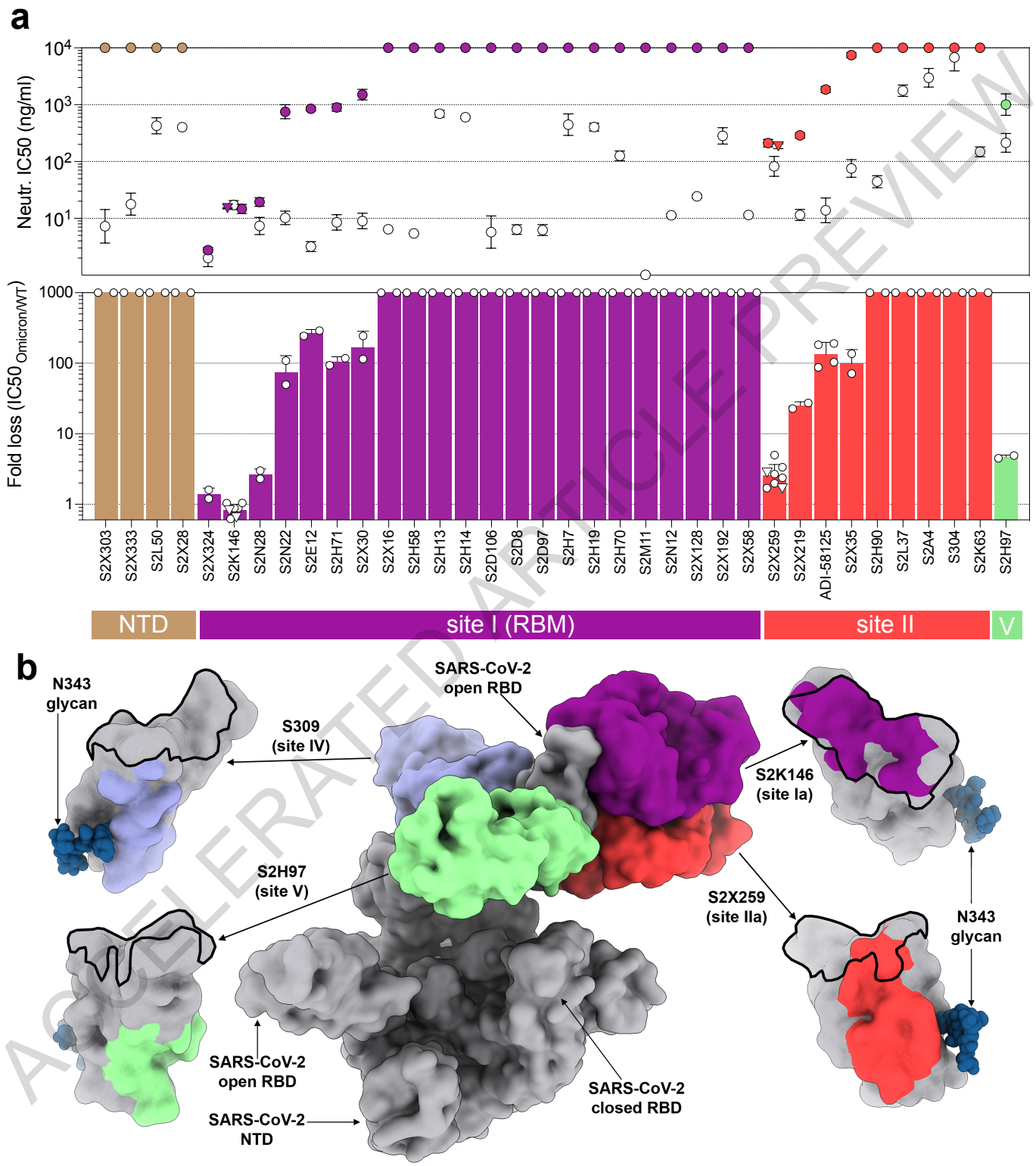

Fig. 4. Neutralization of Omicron SARS-CoV-2 VSV pseudovirus by monoclonal antibodies. a, Mean IC50 values for Omicron (colored as in b) and Wuhan-Hu-1 (white) (top panel), and mean fold change (bottom panel) for 4 NTD mAbs and 32 RBD mAbs. Non-neutralizing IC50 titers and fold change were set to 10^4 and 10^3, respectively. Triangles for S2K146 and S2X259 indicate neutralization of Omicron carrying R346K. Vero E6 used as target cells. Data are representative of n = 2 biologically independent experiments (except for S2K146 and S2X259 where n = 6). **b,** The RBD sites targeted by 4 mAbs cross-neutralizing Omicron are annotated and representative antibodies (the Fv region) bound to S are shown as a composite. Colored surfaces on the RBD depict the epitopes and the RBM is shown as a black outline.

Extended Data Fig. 1

	PANGO	WHO label	Signal peptide and NTD	RBM	S1/S2	S2
VOC	B.1.1.7	Alpha (α)	H69-/ V70-/ Y144-	N501Y	A570D/D614G/P681H	T716I/S982A/D1118H
VOC	B.1.351	Beta (β)	L18F/D80A/D215G/242-244 del	K417N/E484K/N501Y	D614G	A701V
VOC	P.1	Gamma (γ)	L18F/T20N/P26S/D138Y/R190S	K417T/E484K/N501Y	D614G/H655Y	T1027I/V1176F
VOC	B.1.617.2	Delta (δ)	T19R/G142D/E156G/F157-/R158-	L452R/T478K	D614G/P681R	D950N
VOC	B.1.1.529	Omicron (ο)	A67V / Δ69-70 / T95I / G142D/Δ143-145 Δ211/L212I / ins214EPE	G339D / S371L / S373P / S375F / K417N / N440K / G446S / S477N / T478K / E484A / Q493R / G496S / Q498R / N501Y / Y505H	T547K / D614G/ H655Y/ N679K/ P681H	N764K/ D796Y/ N856K/ Q954H/ N969K/ L981F
VOI	C.37	Lambda (λ)	G75V/T76I/246-252del	L452Q/F490S		T859N
VOI	B.1.621	Mu (μ)	T95I/Y144T/Y145S/ins146N	R346K/E484K/N501K	D614G/P681H	D950N
VUM	B.1.617.1	Kappa (κ)	T95I/G142D/E154K	L452R/E484Q	D614G/P681R	Q1071H
VUM	B.1.526	Iota (ι)	L5F/T95I/D253G	E484K	D614G	A701V
VUM	B.1.525	Eta (η)	Q52R/A67V/H69-/V70-/Y144-	E484K	D614G/Q677H	F888L
Former	B.1.429	Epsilon (ε)	S13I/W152C	L452R	D614G	
Former	P.2	Zeta (ζ)		E484K	D614G	
Former	P.3	Theta (θ)	141-143del/242-244del	E484K/N501Y	P681H	S1101Y/E1092K/V1176F

Extended Data Fig. 1. Schematic of mutations landscape in SARS-CoV-2 VOC, VOI and VUM (Variant Under Monitoring). D, deletion: ins, insertion.

Extended Data Fig. 2

a

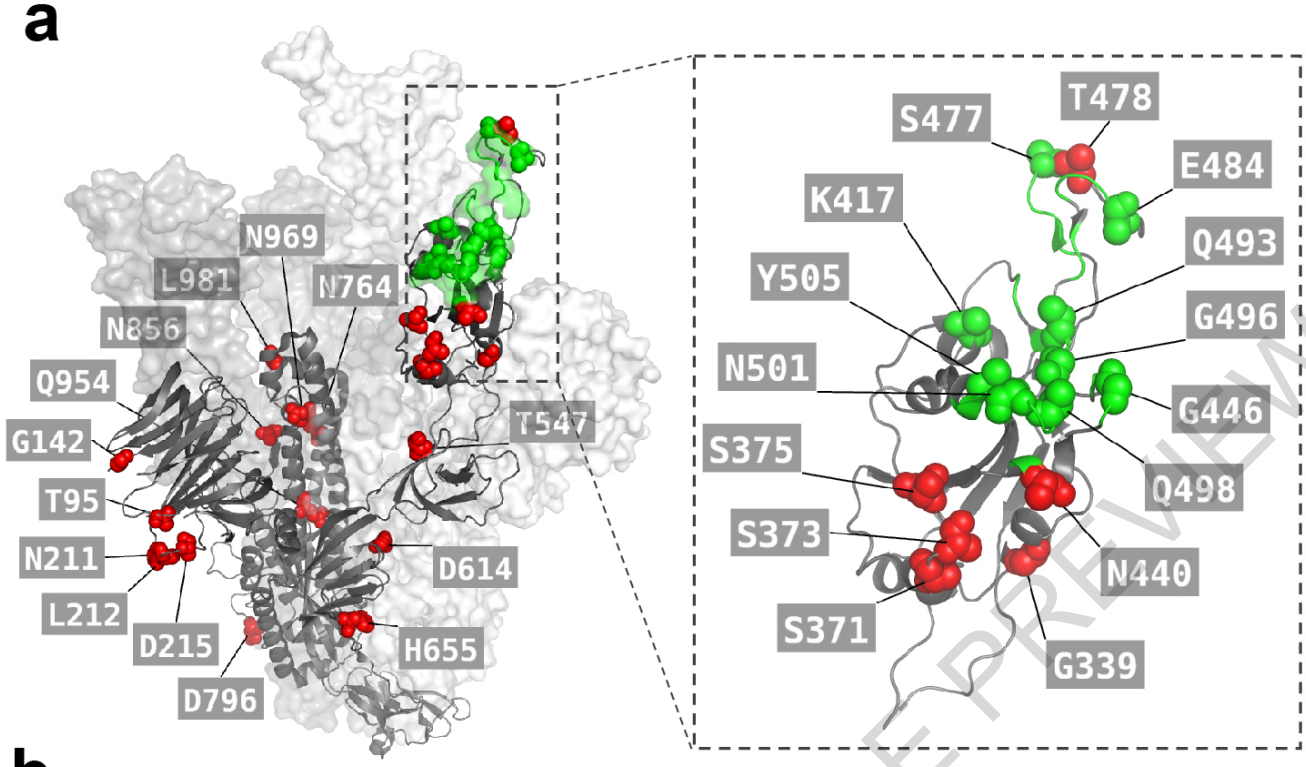

b

Sum of counts (N=12696)	G339	R346	S371	S373	S375	K417	N440	G446	L452	S477	T478	E484	Q493	G496	Q498	N501	Y505	
7410	D		L	P	F					N	K	A	R	S	R	Y	H	Wu-1
2044	D		L	P	F	N	K	S		N	K	A	R	S	R	Y	H	Omicron VOC, as of December 20, 2021
590	D	K	L	P	F					N	K	A	R	S	R	Y	H	
308	D																	
257	D	K	L	P	F	N	K	S		N	K	A	R	S	R	Y	H	
201	D		L	P	F					N	K	A	R	S	R	Y	H	
173						N	K	S		N	K	A	R	S	R	Y	H	
120	D		L	P	F	N				N	K	A	R	S	R	Y	H	
89	D		L	P	F				R	N	K	A	R	S	R	Y	H	
55																		
47	D						K	S		N	K	A	R	S	R	Y	H	
46	D		L	P	F		K	S		N	K	A	R	S	R	Y	H	
40	D		L	P	F		K	S		N	K	A	R	S	R	Y	H	
25	D		L	P	F	N												
22	D	K																
20	D		L	P	F					N	K	A	R	S	R	Y	H	
prevalence (%)	**99.7**	**8.9**	**99.4**	**99.0**	**98.8**	**91.8**	**93.8**	**94.5**	**3.9**	**99.4**	**99.6**	**99.4**	**99.6**	**99.5**	**99.6**	**99.6**	**99.6**	
Alpha (α)																Y		VOC
Beta (β)						N						K				Y		
Gamma (γ)						T						K				Y		
Delta (δ)						*N*			R		K							
Epsilon (ε)									R									VOI
Zeta (ζ)												K						
Eta (η)												K						
Theta (θ)												K				Y		
Iota (ι)												K						
Kappa (κ)									R		Q							
Lambda (λ)									Q									
Mu (μ)		K										K				Y		

Extended Data Fig. 2. **Amino acid substitutions and their prevalence in the Omicron RBD. a,** SARS-CoV-2 S in fully open conformation (PDB: 7K4N) with positions of mutated residues in Omicron highlighted on one protomer in green or red spheres in or outside the ACE2 footprint (ACE2), respectively. RBM is defined by a 6 Å cutoff in the RBD-ACE2 interface[38]. Not all Omicron mutations are shown. **b**, Substitutions and their prevalence in Omicron sequences reported in GISAID as of December 20, 2021 (ambiguous amino acid substitutions are indicated with strikethrough cells). Shown are also the substitutions found in other variants. K417N mutation in Delta is found only in a fraction of sequences.

Extended Data Fig. 3

Sum of counts (N=12696)	A67	H69	V70	T95	L141	G142	V143	Y144	Y145	I210	N211	L212	R214	Wu-1
10271	V	-	-	I		D	-	-	-		-	I	REPE	Omicron, as of Dec. 20, 2021
353	V	-	-	I		D	-	-	-					
336	V	-	-	I		D	-	-	-		-	I		
153	V			I		X								
61	V	-	-	I		D	-	-	-	IIV	R			
43	V	-	-	I	F						-	I	REPE	
42	V			I										
36	V	-	-	I	F						-	I	REPE	
33	V	-	-	I							-	I	REPE	
25	V	-	-	I							-	I		
23	V	-	-	I		D	-	-	-					
prevalence (%)	**99.9**	**99.9**	**99.9**	**99.8**	**0.8**	**98.4**	**99.4**	**99.5**	**99.4**	**0.6**	**99.7**	**99.7**	**93.1**	
Alpha (α)		-	-					-						VOC
Beta (β)														
Gamma (γ)														
Delta (δ)				/		D								
Epsilon (ε)														VOI
Zeta (ζ)														
Eta (η)	V	-	-					-						
Theta (θ)					-	-	-							
Iota (ι)				I										
Kappa (κ)				I		D								
Lambda (λ)														
Mu (μ)				I				T						

Extended Data Fig. 3. **Amino acid substitutions and their prevalence in the Omicron NTD. S**equences reported in GIAID as of December 20, 2021; (ambiguous amino acid substitutions are marked with strikethrough cells). Shown are also the substitutions found in other variants.

Extended Data Fig. 4

Sum of counts (N=12696)	N679	P681	A701	N764	D796	N856	Q954	N969	L981	I1081	D1084	V1264	Wu-1
6039	K	H		K	Y	K	H	K	F				Omicron , as of Dec. 20, 2021
1817	K	H	V	K	Y	K	H	K	F				
1018	K	H			Y	K	H	K	F				
1006	K	H			Y	K	H	K	F				
563	K	H	V		Y	K	H	K	F				
516	K	H		K	Y	K	H	K	F	V			
174	K	H			Y	K	H	K	F	V			
92	K	H			Y	K	H	K	F	V			
89	K	H											
38	K	H		K	Y	K	H	K	F			M	
37	K	H		K	Y	K	H	K	F				
27	K	H			Y	K	H	K	F				
21	K	H				K	H	K	F				
20					Y	K	H	K	F				
20	K	H		K	Y	K	H	K	F		E		
prevalence (%)	99.7	99.7	22.9	99.3	99.8	99.8	99.9	99.8	99.8	7	0.2	0.5	
Alpha (α)		H		I									VOC
Beta (β)			V										
Gamma (γ)													
Delta (δ)		R											
Epsilon (ε)													VOI
Zeta (ζ)													
Eta (η)		H											
Theta (θ)													
Iota (ι)			V										
Kappa (κ)		R											
Lambda (λ)													
Mu (μ)		H											

Extended Data Fig. 4. **Amino acid substitutions and their prevalence in the Omicron S2. S**equences reported in GIAID as of December 20, 2021; (ambiguous amino acid substitutions are marked with strikethrough cells). Shown are also the substitutions found in other variants.

Extended Data Fig. 5

a

	Sarbecovirus			VOC				VOIs
	Clade1	Clade2	Clade3	Alpha	Beta	Gamma	Delta	
A67V								X
H69del	X	X		X				X
V70del	X	X	X	X				X
T95I		X						X
G142D		X						X
V143del								
Y144del	X	X		X				X
Y145del	X	X						X
N211del		X						
L212I								
ins214EPE								
G339D		X						
S371L								
S373P								
S375F								
K417N					X	X		
N440K		X						
G446S	X							
S477N								X
T478K	X	X					X	
E484A					X	X		X
Q493R	X							
G496S								
Q498R								
N501Y				X	X	X		X
Y505H	X							
T547K		X						
D614G				X	X	X	X	X
H655Y			X			X		
N679K								
P681H				X			X	X
N764K								
D796Y	X							
N856K								
Q954H								
N969K								
L981F								

b

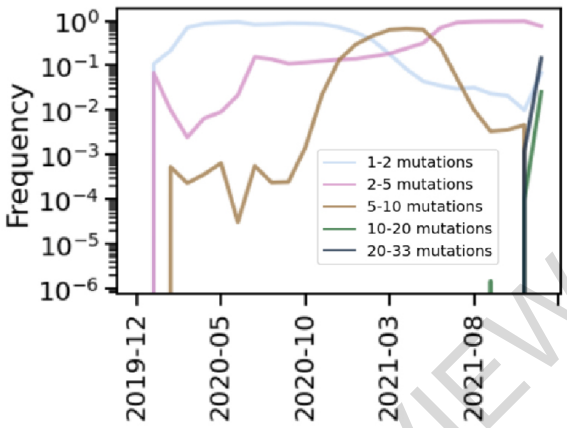

c

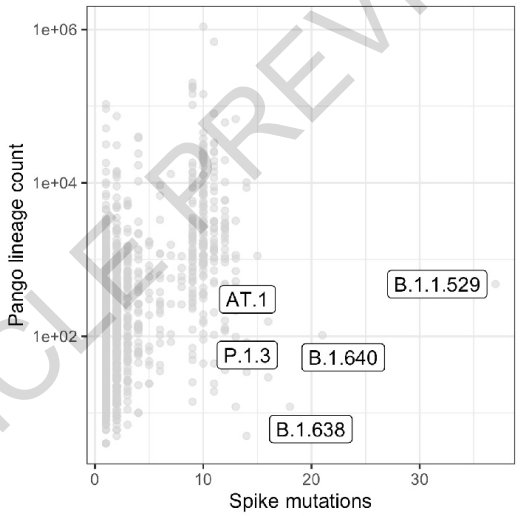

d

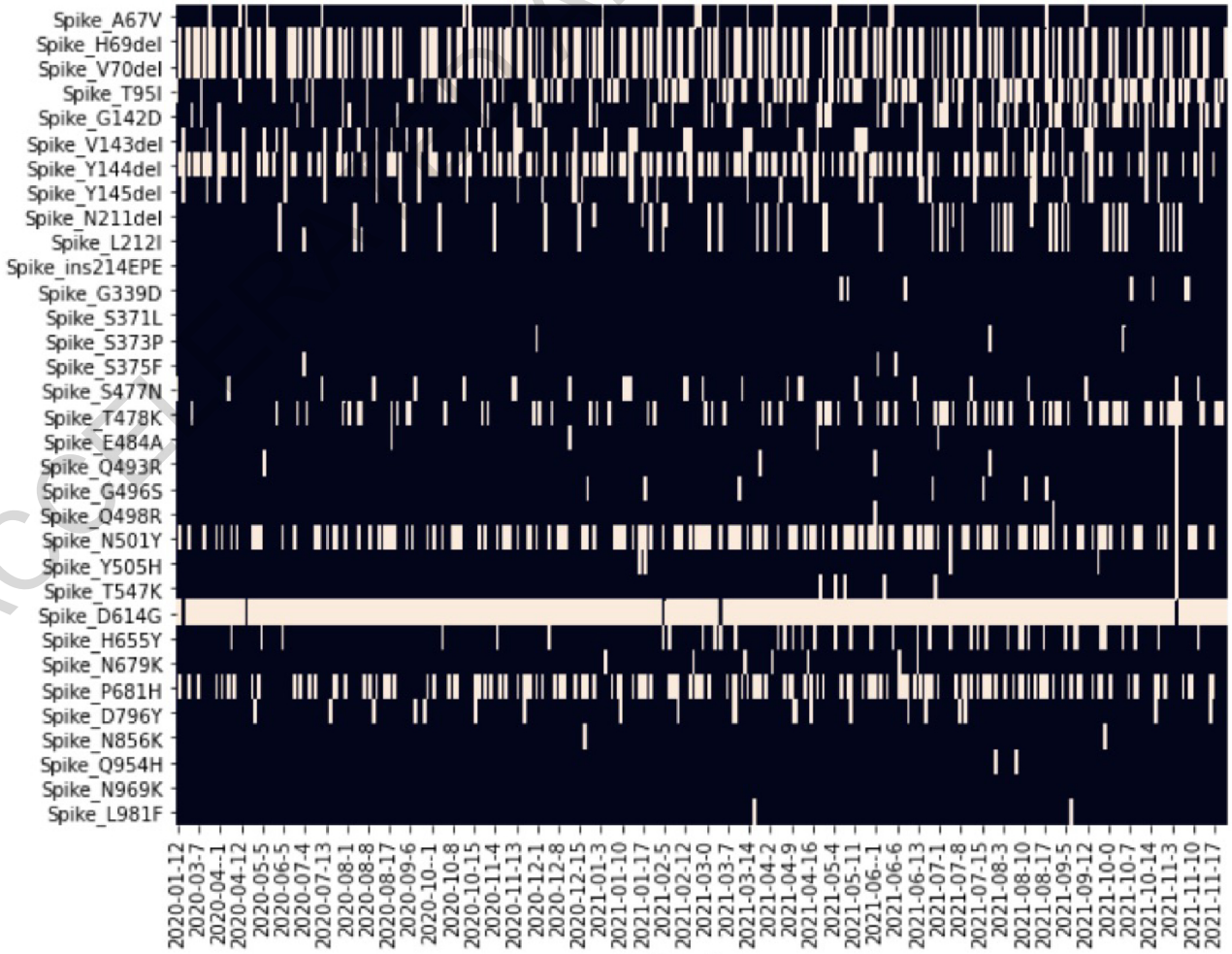

Extended Data Fig. 5. Characteristics of emergent mutations of Omicron. a, Shared mutations of micron with other sarbecovirus and with VOC. **b,** Since the beginning of the pandemic there is a progressive coalescence of Omicron-defining mutations into non-Omicron haplotypes that may carry as many as 10 of the Omicron-defining mutations. **c**, Pango lineages (dots) rarely carry more than 10-15 lineage-defining mutations. **d,** Exceptionally, some non-Omicron haplotypes may carry up to a maximum 19 Omicron-defining mutations. Shown are selected exceptional haplotypes. Spike G142D and Y145del may also be noted as G142del and Y145D.

a

Analyte	Capture format	RBD variant	ka (1/Ms)	kd (1/s)	KD (M)	Rmax (RU)	RBD capture level (RU)
Monomeric Human ACE2	StrepTactin: TwinStrep Tag	**WT**	1.07E+05	0.00627	5.86E-08	101.9	57
		K417N	9.16E+04	0.01763	1.93E-07	98.6	65
		Beta	1.18E+05	0.00293	2.49E-08	111.2	60
		Omicron	8.87E+04	0.00228	2.57E-08	109.1	73
		Alpha	1.17E+05	0.00111	9.56E-09	131.2	64
	Streptavidin :Biotin	**WT**	6.99E+04	0.00644	9.23E-08	82.92	67
		Delta	5.53E+04	0.00425	7.68E-08	79.65	65
Monomeric Mouse ACE2	StrepTactin: TwinStrep Tag	**Omicron**	3.69E+05	0.1782	4.83E-07	95.75	72

b

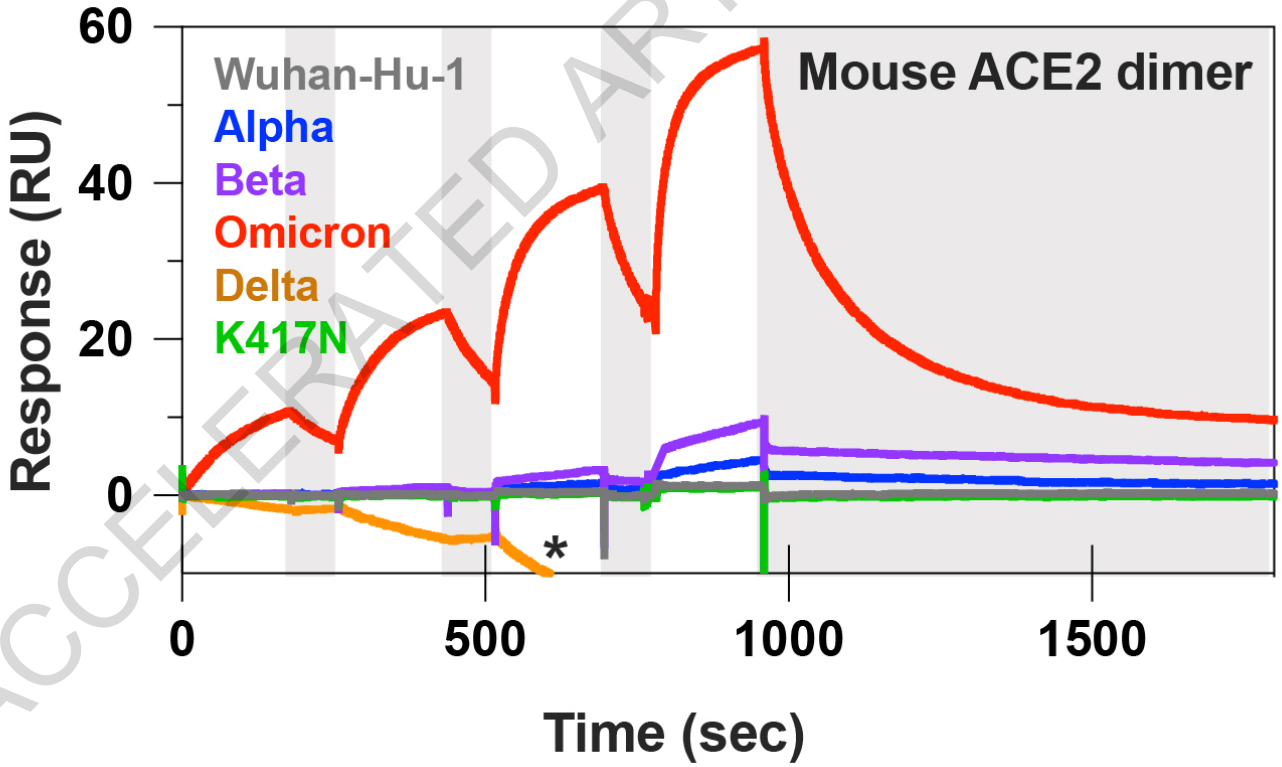

Extended Data Fig. 6. SPR analysis of human and mouse ACE2. a, Full fit results for one representative replicate from each quantifiable SPR dataset with a monomeric analyte (1:1 binding model). **b**, Single-cycle kinetics SPR analysis of dimeric mouse ACE2 binding to six RBD variants. Dimeric ACE2 is injected successively at 33, 100, 300, and 900 nM. White and gray stripes indicate association and dissociation phases, respectively. The asterisk indicates where high concentrations of dimeric mouse ACE2 is non-specifically binding to the sensor chip surface (Delta experiment was performed separately from the other RBD variants, with a different capture tag and chip surface).

Extended Data Fig. 7

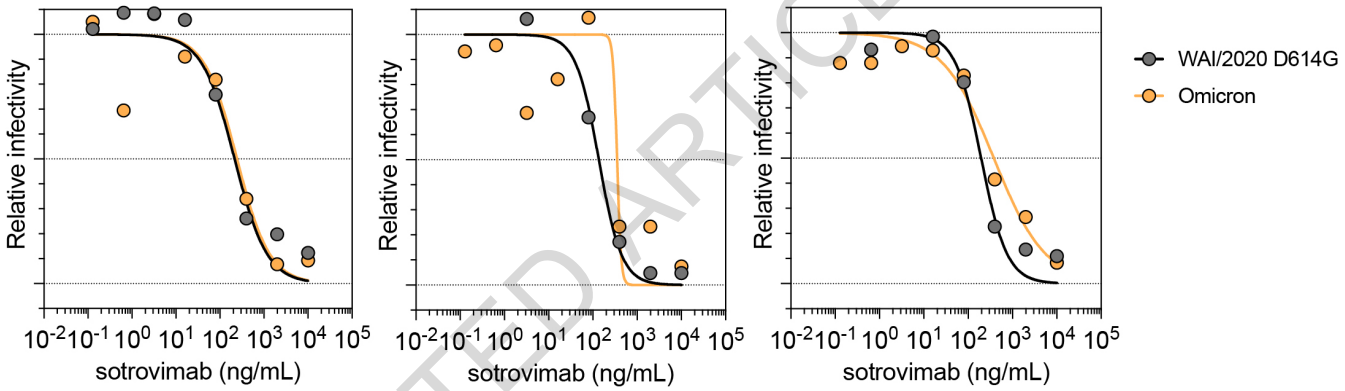

Extended Data Fig. 7. Neutralization of SARS-CoV-2 Omicron strain by sotrovimab in Vero-TMPRSS2 cells. a-f, Neutralization curves in Vero-TMPRSS2 cells comparing the sensitivity of SARS-CoV-2 strains with sotrovimab with WA1/2020 D614G and hCoV-19/USA/WI-WSLH-221686/2021 (an infectious clinical isolate of Omicron from a symptomatic individual in the United States). Shown are three independent experiments performed in technical duplicate is shown.

Extended Data Fig. 8

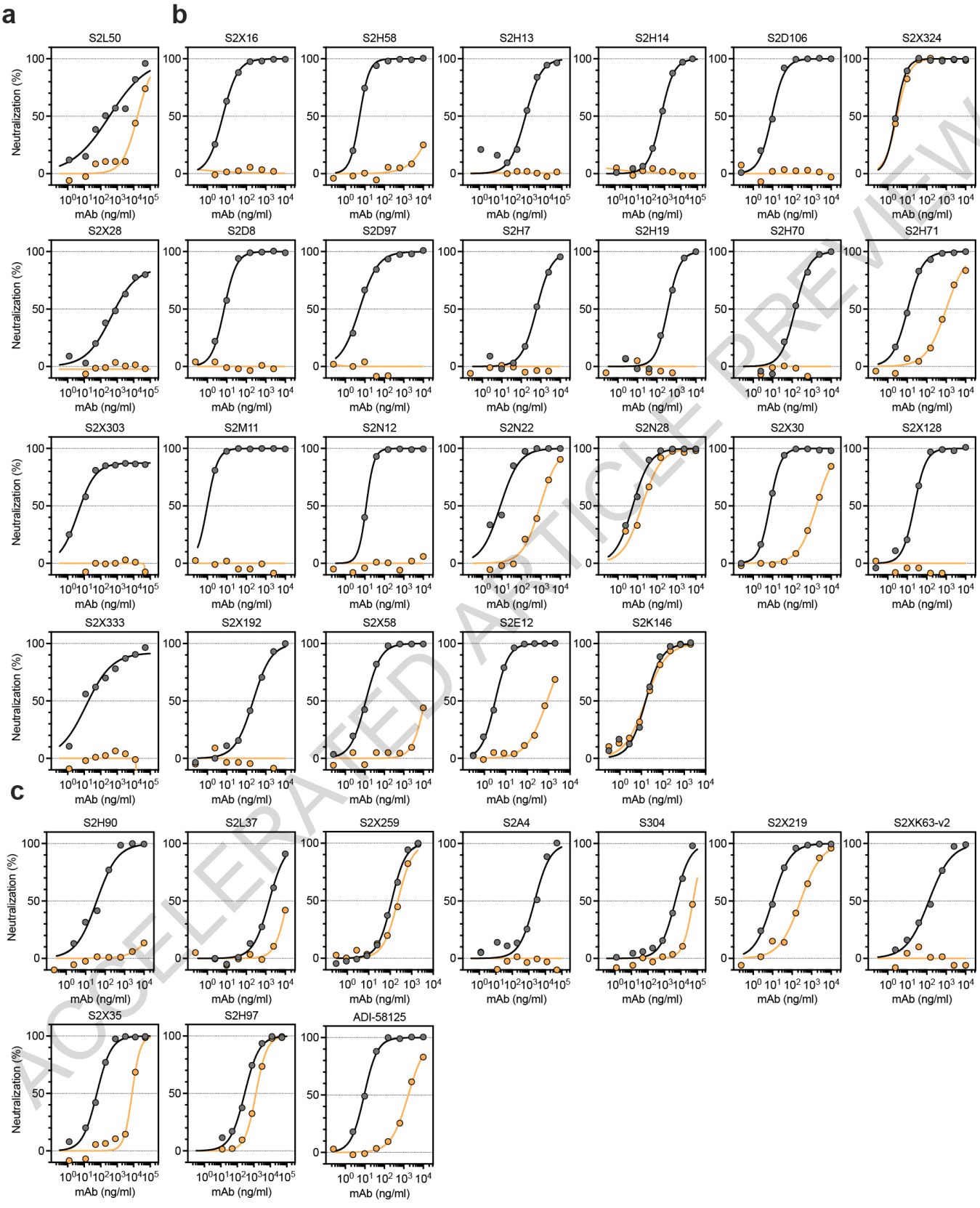

Extended Data Fig. 8. Neutralization of WT (D614) and Omicron SARS-CoV-2 Spike pseudotyped virus by a panel of 36 mAbs. a-c, Neutralization of SARS-CoV-2 VSV pseudoviruses carrying wild-type D614 (grey) or Omicron (orange) S protein by NTD-targeting (**a**) and RBD-targeting (**b-c**) mAbs (**b**, site I; **c**, sites II and V). Data are representative of one independent experiment out of two. Shown is the mean. of 2 technical replicates.

Extended Data Table 1

2-4 weeks after infection/2nd vaccine dose	Dating of SARS-CoV-2 infection	Figure	Nr.	Females	Males	Age (average, range)
Wild type SARS-CoV-2-infected convalescent			**29**	**10**	**19**	**56, 34-73**
Ospedale Luigi Sacco	Mar-Apr 2020	2b	11	1	10	56, 34-73
Swiss volunteers	Mar 2020	2b	1		1	52, 52-52
HAARVI (University of Washington)	Mar-Apr 2020	2a	17	9	8	51, 25-78
Previously infected BNT162b2-vaccinated			**29**	**19**	**10**	**39, 26-56**
Clinica Luganese Moncucco	Mar-Nov 2020	2b	4	3	1	38, 27-54
Ente Ospedaliero Cantonale (EOC)	Mar 2020-Jan 2021	2b	18	14	4	39, 26-56
EOC, dialysis pts	Mar 2020-Jan 2021	2c	7	2	5	69, 48-87
Naïve BNT162b2-vaccinated			**99**	**49**	**50**	**43, 24-67**
Clinica Luganese Moncucco		2b	7	4	3	42, 28-50
Ente Ospedaliero Cantonale (EOC)		2b	18	13	5	43, 24-67
EOC, dialysis pts		2c	55	22	33	74, 29-97
HAARVI (University of Washington)		2a	17	10	7	45, 22-76
Naïve mRNA-1273-vaccinated			**40**	**25**	**15**	
Innovative Research, Novi Michigan (1 week after 2nd dose)		2b	20	14	6	58, 34-74
EOC, dialysis pts		2c	8	2	6	85, 81-92
HAARVI (University of Washington)		2a	14	9	5	47, 23-79
Naïve ChAdOx1-vaccinated						
INGM, Ospedale Maggio Policlinico		2a	17	13	4	38, 29-51
Naïve Sputnik V-vaccinated						
Hospital de Clínicas José de San San Martin, Buenos Aires		2a	11	7	4	42, 30-58
Naïve BBIBP-CorV-vaccinated						
Aga Khan University		2a	13	9	4	30, 25-39

1-19 weeks after 1st vaccine dose		Nr.	Females	Males	Age (average, range)
Naïve Ad26.COV2.S-vaccinated					
HAARVI (University of Washington)	2a	12	6	6	33, 23-60

Total	**250**	**138**	**112**	

Extended Data Table 1. Enrolled donors' demographics. Table shows the characteristics of the individuals in the analyzed cohorts, including gender, age range and type of vaccine received.

Extended Data Table 2

mAb	Domain (site)	VH usage	Source (days after symptom onset)	IC50 Wu-Hu-1 (ng/ml)	IC50 Omicron (ng/ml)	PDB/EMD	Ref.
sotrovimab	RBD (IV)	3-23	SARS-CoV immune	90.6	260	6WPS, 7JX3	2-4,9,40,62,63
					209 (R346K)		
				179 (WA1/2020)	320 (hCoV-19/USA/WI-WSLH-221686/2021)		
VIR-7832*	RBD (IV)	3-23	SARS-CoV immune	53.2	165	6WPS, 7JX3	2-4,9,40,62,63
CT-P59	RBD (I/RBM)	N/A	SARS-CoV-2 immune	4.3	>10'000	7CM4	64,65
COV2-2130	RBD (I/RBM)	3-15	SARS-CoV-2 immune	8.1	2772	7L7E	36,37
COV2-2196	RBD (I/RBM)	1-58	SARS-CoV-2 immune	4.3	>10'000	7L7E, 7L7D	36,37
2130+2196				3.8	418		
REGN10933	RBD (I/RBM)	3–11	SARS-CoV-2 huIg mice	8.9	>10'000	6XDG	31,32,66-68
REGN10987	RBD (I/RBM)	3–30	SARS-CoV-2 immune	25.1	>10'000	6XDG	31,32,66-68
103933+10987				7.2	>10'000		
LY-CoV555	RBD (I/RBM)	1-69	SARS-CoV-2 immune	21.3	>10'000	7KMG	34,35,69,70
LY-CoV016	RBD (I/RBM)	3-66	SARS-CoV-2 immune	59.2	>10'000	7C01	33
555+016				23	>10'000		
S2D106	RBD (I/RBM)	1-69	Hosp. (98)	9.1	>10'000	7R7N	4,38
S2D8	RBD (I/RBM)	3-23	Hosp. (49)	7.3	>10'000		38
S2D97	RBD (I/RBM)	2-5	Hosp. (98)	5.3	>10'000		38
S2E12	RBD (I/RBM)	1-58	Hosp. (51)	3.7	896	7K4N, 7R6X	4,38,40,44
S2H14	RBD (I/RBM)	3-15	Sympt. (17)	625	>10'000	7JX3	4,12,38
S2H19	RBD (I/RBM)	3-15	Sympt. (45)	361	>10'000		38
S2H58	RBD (I/RBM)	1-2	Sympt. (45)	5.4	>10'000		4,38
S2H7	RBD (I/RBM)	3-66	Sympt. (17)	607	>10'000		38
S2H70	RBD (I/RBM)	1-2	Sympt. (45)	145	>10'000		38
S2H71	RBD (I/RBM)	2-5	Sympt. (45)	10.6	993		38
S2M11	RBD (I/RBM)	1-2	Hosp. (46)	1.0	>10'000	7K43	9,38,44
S2N12	RBD (I/RBM)	4-39	Hosp. (51)	11.8	10.8		38
S2N22	RBD (I/RBM)	3-23	Hosp. (51)	8.4	919		38
S2N28	RBD (I/RBM)	3-30	Hosp. (51)	5.8	17.1		38
S2X128	RBD (I/RBM)	1-69-2	Sympt. (75)	23.2	>10'000		38
S2X16	RBD (I/RBM)	1-69	Sympt. (48)	6.2	>10'000		4,38
S2X192	RBD (I/RBM)	1-69	Sympt. (75)	223	>10'000		38
S2X30	RBD (I/RBM)	1-69	Sympt. (48)	7.2	1750		38
S2X324	RBD (I/RBM)	2-5	Sympt. (125)	2.6	3.0		21
S2X58	RBD (I/RBM)	1-46	Sympt. (48)	11.1	>10'000	EMD-24607	4,38
S2K146	RBD (I/RBM)	3-43	Sympt. (35)	14.2	12.6	pending	1
S2H13	RBD (I/RBM)	3-7	Sympt. (17)	628	>10'000	7JV4	4,12
ADI-58125	RBD (II)	3-23	SARS-CoV immune	9.3	1703		71
S2H90	RBD (II)	4-61	Sympt. (81)	37	>10'000		38
S2K63v2	RBD (II)	3-30	Sympt. (118)	129	>10'000		21
S2L37	RBD (II)	3-13	Hosp. (51)	1496	>10'000		21
S2X259	RBD (II)	1-69	Sympt. (75)	81.8	193.6	7RA8, 7M7W	3
S2X35	RBD (II)	1-18	Sympt. (48)	58.6	7999	7R6W	4,12
S2X219	RBD (II)	3-53	Sympt. (75)	9.8	268.3		
S304	RBD (II)	3-13	SARS-CoV immune	4603	>10'000	7JX3	4,12
S2A4	RBD (II)	3-7	Hosp. (24)	2285	>10'000	7JVC	12
S2H97	RBD (V)	5-51	Sympt. (81)	280	1368	7M7W	4
S2L50	NTD (i)	4-59	Hosp. (52)	338	>10'000		45
S2X28	NTD (i)	3-30	Sympt. (48)	423	>10'000	EMD-23584	45
S2X303	NTD (i)	2-5	Sympt. (125)	4.5	>10'000	7SOF, 7SOE	9,45
S2X333	NTD (i)	3-33	Sympt. (125)	13	>10'000	7LXW, 7LXY	9,40,45

Extended Data Table 2. Properties of tested mAbs. Tables shows details of the full set of mAbs characterized for their neutralizing activity in Fig. 3 and 4, including specificity, V gene usage for the heavy chain, original source, IC50 values, accession codes of available structures and relevant references.

MATERIALS AND METHODS

Cell lines

Cell lines used in this study were obtained from ATCC (HEK293T and Vero E6), ThermoFisher Scientific (Expi CHO cells, FreeStyle™ 293-F cells and Expi293F™ cells), Lenti-X 293T cells (Takara) or generated in-house (Vero E6/TMPRSS2)[40]. Vero-TMPRSS2[51] cells were cultured at 37°C in Dulbecco's Modified Eagle medium (DMEM) supplemented with 10% fetal bovine serum (FBS), 10 mM HEPES pH 7.3, and 100 U/ml of penicillin–streptomycin and supplemented with 5 µg/mL of blasticidin. None of the cell lines used was authenticated. Cell lines were routinely tested for mycoplasma contamination.

Omicron prevalence analysis

The viral sequences and the corresponding metadata were obtained from GISAID EpiCoV project (https://www.gisaid.org/). Analysis was performed on sequences submitted to GISAID up to Dec 09, 2021. S protein sequences were either obtained directly from the protein dump provided by GISAID or, for the latest submitted sequences that were not incorporated yet in the protein dump at the day of data retrieval, from the genomic sequences with the exonerate[52] 2 2.4.0–haf93ef1_3 (https://quay.io/repository/biocontainers/exonerate?tab=tags) using protein to DNA alignment with parameters -m protein2dna –refine full –minintron 999999 –percent 20 and using accession YP_009724390.1 as a reference. Multiple sequence alignment of all human spike proteins was performed with mafft[53] 7.475–h516909a_0 (https://quay.io/repository/biocontainers/mafft?tab=tags) with parameters –auto –reorder – keeplength –addfragments using the same reference as above. S sequences that contained >10% ambiguous amino acid or that were < than 80% of the canonical protein length were discarded. Figures were generated with R 4.0.2 (https://cran.r-project.org/) using ggplot2 3.3.2 and sf 0.9-7 packages. To identify each mutation prevalence, missingness (or ambiguous amino acids) was taken into account in both nominator and denominator.

Monoclonal Antibodies

Sotrovimab and VIR-7832 (VIR-7832[54] is derived from sotrovimab, Fc further engineered to carry GAALIE) were produced at WuXi Biologics (China). Antibody VH and VL sequences for mAbs COV2-2130 (PDB ID 7L7E), COV2-2196 (PDB ID 7L7E, 7L7D), REGN10933 (PDB ID 6XDG), REGN10987 (PDB ID 6XDG) and ADI-58125 (PCT application WO2021207597, seq. IDs 22301 and 22311) were subcloned into heavy chain (human IgG1) and the corresponding light chain (human IgKappa, IgLambda) expression vectors respectively and produced in transiently transfected Expi-CHO-S cells (Thermo Fisher, #A29133) at 37°C and 8% CO2. Cells were transfected using ExpiFectamine. Transfected cells were supplemented 1 day after transfection with ExpiCHO Feed and ExpiFectamine CHO Enhancer. Cell culture supernatant was collected eight days after transfection and filtered through a 0.2 µm filter. Recombinant antibodies were affinity purified on an ÄKTA Xpress FPLC device using 5 mL HiTrap™ MabSelect™ PrismA columns followed by buffer exchange to Histidine buffer (20 mM Histidine, 8% sucrose, pH 6) using HiPrep 26/10 desalting columns. Antibody VH and VL sequences for LY-CoV555, LY-CoV016, and CT-P59 were obtained from PDB IDs 7KMG, 7C01 and 7CM4, respectively and mAbs were produced as recombinant IgG1 by ATUM. The remaining mAbs were discovered at VIR and have been produced as recombinant IgG1 in Expi-CHO-S cells as described above. The identity of the produced mAbs was confirmed by LC-MS analysis.

IgG mass quantification by LC/MS intact protein mass analysis

Fc N-linked glycan from mAbs were removed by PNGase F after overnight non-denaturing reaction at room temperature. Deglycosylated protein (4 µg) was injected to the LC-MS system to acquire intact MS signal. Thermo MS (Q Exactive Plus Orbitrap) was used to acquire intact protein mass under denaturing condition with m/z window from 1,000 to 6,000. BioPharma Finder 3.2 software was used to deconvolute the raw m/z data to protein average mass. The theoretical mass for each mAb was calculated with GPMAW 10.10 software. Post-translational modifications such as N-terminal pyroglutamate cyclization, C-terminal lysine cleavage, and formation of 16-18 disulfide bonds were added into the calculation.

Sample donors

Samples were obtained from SARS-CoV-2 recovered and vaccinated individuals under study protocols approved by the local Institutional Review Boards (Canton Ticino Ethics Committee, Switzerland, Comitato Etico Milano Area 1). All donors provided written informed consent for the use of blood and blood derivatives (such as PBMCs, sera or plasma) for research. Samples were collected 14-28 days after symptoms onset and 14-28 days or 7-10 months after vaccination. Convalescent plasma, Ad26.COV2.S, mRNA-1273 and BNT162b2 samples were obtained from the HAARVI study approved by the University of Washington Human Subjects Division Institutional Review Board (STUDY00000959). AZD1222 samples were obtained from INGM, Ospedale Maggio Policlinico of Milan and approved by the local review board Study Polimmune. Sputnik V samples were obtained from healthcare workers at the hospital de Clínicas "José de San Martín", Buenos Aires, Argentina. Sinopharm vaccinated individuals were enrolled from Aga Khan University under IRB of UWARN study.

Serum/plasma and mAbs pseudovirus neutralization assays

VSV pseudovirus generation used on Vero E6 cells

The plasmid encoding the Omicron SARS-CoV-2 S variant was generated by overlap PCR mutagenesis of the wild-type plasmid, pcDNA3.1(+)-spike-D19[55]. Replication defective VSV pseudovirus expressing SARS-CoV-2 spike proteins corresponding to the ancestral Wuhan-Hu-1 virus and the Omicron VOC were generated as previously described[46] with some modifications. Lenti-X 293T cells (Takara) were seeded in 15-cm^2 dishes at a density of 10e6 cells per dish and the following day transfected with 25 µg of spike expression plasmid with TransIT-Lenti (Mirus, 6600) according to the manufacturer's instructions. One day post-transfection, cells were infected with VSV-luc (VSV-G) with an MOI 3 for 1 h, rinsed three times with PBS containing Ca2+/Mg2+, then incubated for additional 24 h in complete media at 37°C. The cell supernatant was clarified by centrifugation, aliquoted, and frozen at -80°C.

VSV pseudovirus generation used on Vero E6-TMPRSS2 cells

Comparison of Omicron SARS-CoV-2 S VSV to SARS-CoV-2 G614 S (YP 009724390.1) VSV and Beta S VSV used pseudotyped particles prepared as described previously[9,56]. Briefly, HEK293T cells in DMEM supplemented with 10% FBS, 1% PenStrep seeded in 10-cm dishes were transfected with the plasmid encoding for the corresponding S glycoprotein using lipofectamine 2000 (Life Technologies) following the manufacturer's instructions. One day post-transfection, cells were infected with VSV(G*ΔG-luciferase)[57] and after 2 h were washed five times with DMEM before adding medium supplemented with anti-VSV-G antibody (I1- mouse hybridoma supernatant, CRL- 2700, ATCC). Virus pseudotypes were harvested 18-24 h post-inoculation, clarified by centrifugation at 2,500 x g for 5 min, filtered through a 0.45 µm cut off membrane, concentrated 10 times with a 30 kDa cut off membrane, aliquoted and stored at -80°C.

VSV pseudovirus neutralization

Assay performed using Vero E6 cells

Vero-E6 were grown in DMEM supplemented with 10% FBS and seeded into clear bottom white 96 well plates (PerkinElmer, 6005688) at a density of 20,000 cells per well. The next day, mAbs or plasma were serially diluted in pre-warmed complete media, mixed with pseudoviruses and incubated for 1 h at 37°C in round bottom polypropylene plates. Media from cells was aspirated and 50 µl of virus-mAb/plasma complexes were added to cells and then incubated for 1 h at 37°C. An additional 100 µL of prewarmed complete media was then added on top of complexes and cells incubated for an additional 16-24 h. Conditions were tested in duplicate wells on each plate and eight wells per plate contained untreated infected cells (defining the 0% of neutralization, "MAX RLU" value) and infected cells in the presence of S309 and S2X259 at 20 µg/ml each (defining the 100% of neutralization, "MIN RLU" value). Virus-mAb/plasma-containing media was then aspirated from cells and 100 µL of a 1:2 dilution of SteadyLite Plus (Perkin Elmer, 6066759) in PBS with Ca^{++} and Mg^{++} was added to cells. Plates were incubated for 15 min at room temperature and then were analyzed on the Synergy-H1 (Biotek). Average of Relative light units (RLUs) of untreated infected wells (MAX RLU_{ave}) was subtracted by the average of MIN RLU (MIN RLU_{ave}) and used to normalize percentage of neutralization of individual RLU values of experimental data according to the following formula: $(1-(RLU_x - \text{MIN } RLU_{ave}) / (\text{MAX } RLU_{ave} - \text{MIN } RLU_{ave})) \times 100$. Data were analyzed and visualized with Prism (Version 9.1.0). IC50 (mAbs) and ID50 (plasma) values were calculated from the interpolated value from the log(inhibitor) versus response, using variable slope (four parameters) nonlinear regression with an upper constraint of ≤100, and a lower constrain equal to 0. Each neutralization experiment was conducted on two independent experiments, i.e., biological replicates, where each biological replicate contains a technical duplicate. IC50 values across biological replicates are presented as arithmetic mean ± standard deviation. The loss or gain of neutralization potency across spike variants was calculated by dividing the variant IC50/ID50 by the parental IC50/ID50 within each biological replicate, and then visualized as arithmetic mean ± standard deviation.

Assay performed using Vero E6-TMPRSS2 cells

VeroE6-TMPRSS2 were cultured in DMEM with 10% FBS (Hyclone), 1% PenStrep and 8 µg/mL puromycin (to ensure retention of TMPRSS2) with 5% CO_2 in a 37°C incubator (ThermoFisher). Cells were trypsinized using 0.05% trypsin and plated to be at 90% confluence the following day. In an empty half-area 96-well plate, a 1:3 serial dilution of sera was made in DMEM and diluted pseudovirus was then added and incubated at room temperature for 30-60 min before addition of the sera-virus mixture to the cells at 37°C. 2 hours later, 40 µL of a DMEM solution containing 20% FBS and 2% PenStrep (ThermoFisher, 10,000 units/mL of penicillin and 10,000 µg/mL of streptomycin when undiluted) was added to each well. After 17-20 hours, 40 µL/well of One-Glo-EX substrate (Promega) was added to the cells and incubated in the dark for 5-10 min prior to reading on a BioTek plate reader. Measurements were done at least in duplicate using distinct batches of pseudoviruses and one representative experiment is shown. Relative luciferase units were plotted and normalized in Prism (GraphPad). Nonlinear regression of log(inhibitor) versus normalized response was used to determine IC_{50} values from curve fits. Normality was tested using the D'Agostino-Pearson test and in the absence of a normal distribution, Kruskal-Wallis tests were used to compare two groups to determine whether differences reached statistical significance. Fold changes were determined by comparing individual IC_{50} and then averaging the individual fold changes for reporting.

Focus reduction neutralization test

The WA1/2020 strain with a D614G substitution was described previously[58]. The B.1.1.529 isolate (hCoV-19/USA/WI-WSLH-221686/2021) was obtained from a nasal swab and passaged on Vero-TMPRSS2 cells as described[59]. The B.1.1.529 isolate was sequenced (GISAID: EPI_ISL_7263803) to confirm the stability of substitutions. All virus experiments were performed in an approved biosafety level 3 (BSL-3) facility.

Serial dilutions of sotrovimab were incubated with 10^2 focus-forming units (FFU) of SARS-CoV-2 (WA1/2020 D614G or B.1.1.529) for 1 h at 37°C. Antibody-virus complexes were added to Vero-TMPRSS2 cell monolayers in 96-well plates and incubated at 37°C for 1 h. Subsequently, cells were overlaid with 1% (w/v) methylcellulose in MEM. Plates were harvested at 30 h (WA1/2020 D614G on Vero-TMPRSS2 cells) or 70 h (B.1.1.529 on Vero-TMPRSS2 cells) later by removal of overlays and fixation with 4% PFA in PBS for 20 min at room temperature. Plates with WA1/2020 D614G were washed and sequentially incubated with an oligoclonal pool of SARS2-2, SARS2-11, SARS2-16, SARS2-31, SARS2-38, SARS2-57, and SARS2-71[60] anti-S antibodies. Plates with B.1.1.529 were additionally incubated with a pool of mAbs that cross-react with SARS-CoV-1 and bind a CR3022-competing epitope on the RBD[61]. All plates were subsequently stained with HRP-conjugated goat anti-mouse IgG (Sigma, A8924) in PBS supplemented with 0.1% saponin and 0.1% bovine serum albumin. SARS-CoV-2-infected cell foci were visualized using TrueBlue peroxidase substrate (KPL) and quantitated on an ImmunoSpot microanalyzer (Cellular Technologies). Antibody-dose response curves were analyzed using non-linear regression analysis with a variable slope (GraphPad Software), and the half-maximal inhibitory concentration (IC_{50}) was calculated.

VSV pseudovirus entry assays using mouse ACE2

HEK293T (293T) cells (ATCC CRL-11268) were cultured in 10% FBS, 1% PenStrep DMEM at 37°C in a humidified 8% CO_2 incubator. Transient transfection of mouse ACE2 in 293T cells was done 18-24 hours prior to infection using Lipofectamine 2000 (Life Technologies) and an HDM plasmid containing full length Mouse ACE2 (GenBank: Q8R010, synthesized by GenScript) in OPTIMEM. After 5 hr incubation at 37°C in a humidified 8% CO_2 incubator, DMEM with 10% FBS was added and cells were incubated at 37°C in a humidified 8% CO_2 incubator for 18-24 hr. Immediately prior to infection, 293T cells with transient expression of mouse ACE2 were washed with DMEM 1x, then plated with pseudovirus at a 1:75 dilution in DMEM. Infection in DMEM was done with cells between 60-80% confluence for 2.5 hr prior to adding FBS and PenStrep to final concentrations of 10% and 1%, respectively. Following 18-24 hr of infection, One-Glo-EX (Promega) was added to the cells and incubated in the dark for 5 min before reading on a Synergy H1 Hybrid Multi-Mode plate reader (Biotek). Cell entry levels of pseudovirus generated on different days (biological replicates) were plotted in GraphPad Prism as individual points, and average cell entry across biological replicates was calculated as the geometric mean.

Recombinant RBD protein production

SARS-CoV-2 RBD proteins for SPR binding assays (residues 328-531 of S protein from GenBank NC_045512.2 with N-terminal signal peptide and C-terminal thrombin cleavage site-TwinStrep-8xHis-tag) were expressed in Expi293F (Thermo Fisher Scientific) cells at 37°C and 8% CO2. Transfections were performed using the ExpiFectamine 293 Transfection Kit (Thermo Fisher Scientific). Cell culture supernatants were collected two to four days after transfection and supplemented with 10x PBS to a final concentration of 2.5x PBS (342.5 mM NaCl, 6.75 mM KCl and 29.75 mM phosphates). SARS-CoV-2

RBDs were purified using cobalt-based immobilized metal affinity chromatography followed by buffer exchange into PBS using a HiPrep 26/10 desalting column (Cytiva) or, for the 2nd batch of Omicron RBD used for SPR, a Superdex 200 Increase 10/300 GL column (Cytiva).
The SARS-CoV-2 Wuhan-Hu-1 and Delta (B.1.617.2) RBD-Avi constructs were synthesized by GenScript into pcDNA3.1- with an N-terminal mu-phosphatase signal peptide and a C-terminal octa-histidine tag, flexible linker, and avi tag (GHHHHHHHHGGSSGLNDIFEAQKIEWHE). The boundaries of the construct are N-$_{328}$RFPN$_{331}$ and $_{528}$KKST$_{531}$-C[9,14]. Proteins were produced in Expi293F cells (ThermoFisher Scientific) grown in suspension using Expi293 Expression Medium (ThermoFisher Scientific) at 37°C in a humidified 8% CO_2 incubator rotating at 130 rpm. Cells grown to a density of 3 million cells per mL were transfected using the ExpiFectamine 293 Transfection Kit (ThermoFisher Scientific) and cultivated for 3-5 days. Proteins were purified from clarified supernatants using a nickel HisTrap HP affinity column (Cytiva) and washed with ten column volumes of 20 mM imidazole, 25 mM sodium phosphate pH 8.0, and 300 mM NaCl before elution on a gradient to 500 mM imidazole. Proteins were biotinylated overnight using the BirA Biotin-Protein Ligase Kit (Avidity) and purified again using the HisTrapHP affinity column. After a wash and elution as before, proteins were buffer exchanged into 20 mM sodium phosphate pH 8 and 100 mM NaCl, and concentrated using centrifugal filters (Amicon Ultra) before being flash frozen.

Recombinant production of ACE2 orthologs

Recombinant human ACE2 (residues 19-615 from Uniprot Q9BYF1 with a C-terminal AviTag-10xHis-GGG-tag, and N-terminal signal peptide) was produced by ATUM. Protein was purified via Ni Sepharose resin followed by isolation of the monomeric hACE2 by size exclusion chromatography using a Superdex 200 Increase 10/300 GL column (Cytiva) pre-equilibrated with PBS. The mouse (*Mus musculus)* ACE2 ectodomain construct (GenBank: Q8R0I0) was synthesized by GenScript and placed into a pCMV plasmid. The domain boundaries for the ectodomain are residues 19-615. The native signal tag was identified using SignalP-5.0 (residues 1-18) and replaced with a N-terminal mu-phosphatase signal peptide. This construct was then fused to a sequence encoding thrombin cleavage site and a human Fc fragment or a 8x His tag at the C-terminus. ACE2-Fc and ACE2 His constructs were produced in Expi293 cells (Thermo Fisher A14527) in Gibco Expi293 Expression Medium at 37°C in a humidified 8% CO2 incubator rotating at 130 rpm. The cultures were transfected using PEI-25K (Polyscience) with cells grown to a density of 3 million cells per mL and cultivated for 4-5 days. Proteins were purified from clarified supernatants using a 1 mL HiTrap Protein A HP affinity column (Cytiva) or a 1 mL HisTrap HP affinity column (Cytiva), concentrated and flash frozen in 1x PBS, pH 7.4 (10 mM Na2HPO4, 1.8 mM KH2PO4, 2.7 mM KCl, 137 mM NaCl).

ACE2 binding measurements using surface plasmon resonance

Measurements were performed using a Biacore T200 instrument, in triplicate for monomeric human and mouse ACE2 and duplicate for dimeric mouse ACE2. A CM5 chip covalently immobilized with StrepTactin XT (IBA LifeSciences) was used for surface capture of TwinStrepTag-containing RBDs (Wuhan-Hu-1, Alpha, Beta, Omicron, K417N) and a Cytiva Biotin CAPture Kit was used for surface capture of biotinylated RBDs (Delta and Wuhan-Hu-1 used for fold-change comparison to Delta). Two different batches of Omicron RBD were used for the experiments. Running buffer was HBS-EP+ pH 7.4 (Cytiva) and measurements were performed at 25℃. Experiments were performed with a 3-fold dilution series of human ACE2 (300, 100, 33, 11 nM) or mouse ACE2 (900, 300, 100, 33 nM) and were run as single-cycle kinetics. Monomeric ACE2 binding data were double reference-subtracted and fit to a 1:1

binding model using Biacore Evaluation software. High concentrations of dimeric mouse ACE2 exhibited significant binding to the CAP sensor chip reference flow cell.

Statistical analysis

Neutralization measurements were performed in duplicate and relative luciferase units were converted to percent neutralization and plotted with a non-linear regression model to determine IC50/ID50 values using GraphPad PRISM software (version 9.0.0). Comparisons between two groups of paired two-sided data were made with Wilcoxon rank test.

Data availability

Materials generated in this study will be made available on request and may require a material transfer agreement. GISAID (www.gisaid.org) data access requires registration. Note: after consulting with the local Ethical authority, due to health and data protection laws relating to the demographic and clinical information contained in the manuscript, we will not be able to fully comply with the requirement to share demographic and clinical data of individual patients/donors in this study.

REFERENCES

1 Park, Y. J. *et al.* Antibody-mediated broad sarbecovirus neutralization through ACE2 molecular mimicry. *bioRxiv*, doi:10.1101/2021.10.13.464254 (2021).

2 Pinto, D. *et al.* Cross-neutralization of SARS-CoV-2 by a human monoclonal SARS-CoV antibody. *Nature* **583**, 290-295, doi:10.1038/s41586-020-2349-y (2020).

3 Tortorici, M. A. *et al.* Broad sarbecovirus neutralization by a human monoclonal antibody. *Nature* **597**, 103-108, doi:10.1038/s41586-021-03817-4 (2021).

4 Starr, T. N. *et al.* SARS-CoV-2 RBD antibodies that maximize breadth and resistance to escape. *Nature* **597**, 97-102, doi:10.1038/s41586-021-03807-6 (2021).

5 Telenti, A. *et al.* After the pandemic: perspectives on the future trajectory of COVID-19. *Nature* **596**, 495-504, doi:10.1038/s41586-021-03792-w (2021).

6 Wang, P. *et al.* Antibody resistance of SARS-CoV-2 variants B.1.351 and B.1.1.7. *Nature* **593**, 130-135, doi:10.1038/s41586-021-03398-2 (2021).

7 Chen, R. E. *et al.* Resistance of SARS-CoV-2 variants to neutralization by monoclonal and serum-derived polyclonal antibodies. *Nat Med* **27**, 717-726, doi:10.1038/s41591-021-01294-w (2021).

8 Corti, D., Purcell, L. A., Snell, G. & Veesler, D. Tackling COVID-19 with neutralizing monoclonal antibodies. *Cell* **184**, 3086-3108, doi:10.1016/j.cell.2021.05.005 (2021).

9 McCallum, M. & Walls, A. C. Molecular basis of immune evasion by the Delta and Kappa SARS-CoV-2 variants. *Science* (2021).

10 Mlcochova, P. *et al.* SARS-CoV-2 B.1.617.2 Delta variant replication and immune evasion. *Nature* **599**, 114-119, doi:10.1038/s41586-021-03944-y (2021).

11 Sheikh, A. *et al.* SARS-CoV-2 Delta VOC in Scotland: demographics, risk of hospital admission, and vaccine effectiveness. *Lancet* **397**, 2461-2462, doi:10.1016/S0140-6736(21)01358-1 (2021).

12 Piccoli, L. *et al.* Mapping Neutralizing and Immunodominant Sites on the SARS-CoV-2 Spike Receptor-Binding Domain by Structure-Guided High-Resolution Serology. *Cell* **183**, 1024-1042 e1021, doi:10.1016/j.cell.2020.09.037 (2020).

13 Greaney, A. J. *et al.* Comprehensive mapping of mutations in the SARS-CoV-2 receptor-binding domain that affect recognition by polyclonal human plasma antibodies. *Cell Host Microbe* **29**, 463-476 e466, doi:10.1016/j.chom.2021.02.003 (2021).

14 Walls, A. C. *et al.* Structure, Function, and Antigenicity of the SARS-CoV-2 Spike Glycoprotein. *Cell* **181**, 281-292 e286, doi:10.1016/j.cell.2020.02.058 (2020).

15 Cele, S. *et al.* SARS-CoV-2 Omicron has extensive but incomplete escape of Pfizer BNT162b2 elicited neutralization and requires ACE2 for infection. *medRxiv* (2021).

16 Wilhelm, A. *et al.* Reduced Neutralization of SARS-CoV-2 Omicron Variant by Vaccine Sera and monoclonal antibodies. *medRxiv*, doi:10.1101/2021.12.07.21267432 (2021).

17 Andrews, N. *et al.* Effectiveness of COVID-19 vaccines against Omicron variant of concern. *https://khub.net* (2021).

18 Cao, Y. R. *et al.* B.1.1.529 escapes the majority of SARS-CoV-2 neutralizing antibodies of diverse epitopes. doi:10.1101/2021.12.07.470392 (2021).

19 Leist, S. R. *et al.* A Mouse-Adapted SARS-CoV-2 Induces Acute Lung Injury and Mortality in Standard Laboratory Mice. *Cell* **183**, 1070-1085 e1012, doi:10.1016/j.cell.2020.09.050 (2020).

20 Dinnon, K. H., 3rd *et al.* A mouse-adapted model of SARS-CoV-2 to test COVID-19 countermeasures. *Nature* **586**, 560-566, doi:10.1038/s41586-020-2708-8 (2020).
21 Collier, D. A. *et al.* Sensitivity of SARS-CoV-2 B.1.1.7 to mRNA vaccine-elicited antibodies. *Nature* **593**, 136-141, doi:10.1038/s41586-021-03412-7 (2021).
22 Starr, T. N. *et al.* Deep Mutational Scanning of SARS-CoV-2 Receptor Binding Domain Reveals Constraints on Folding and ACE2 Binding. *Cell* **182**, 1295-1310 e1220, doi:10.1016/j.cell.2020.08.012 (2020).
23 Shuai, H. *et al.* Emerging SARS-CoV-2 variants expand species tropism to murines. *EBioMedicine* **73**, 103643, doi:10.1016/j.ebiom.2021.103643 (2021).
24 Pan, T. *et al.* Infection of wild-type mice by SARS-CoV-2 B.1.351 variant indicates a possible novel cross-species transmission route. *Signal Transduct Target Ther* **6**, 420, doi:10.1038/s41392-021-00848-1 (2021).
25 Hoffmann, M. *et al.* The Omicron variant is highly resistant against antibody-mediated neutralization – implications for control of the COVID-19 pandemic. *bioRxiv*, doi:10.1101/2021.12.12.472286 (2021).
26 Nicholis, J. & Chan Chi-wai, M. HKUMed finds Omicron SARS-CoV-2 can infect faster and better than Delta in human bronchus but with less severe infection in lung. *www.med.hku.hk/en/news/press/20211215-omicron-sars-cov-2-infection.* (2021).
27 Bassi, J. *et al.* Poor neutralization and rapid decay of antibodies to SARS-CoV-2 variants in vaccinated dialysis patients. *medRxiv*, doi:10.1101/2021.10.05.21264054v2 (2021).
28 Khoury, D. S. *et al.* Neutralizing antibody levels are highly predictive of immune protection from symptomatic SARS-CoV-2 infection. *Nat Med* **27**, 1205-1211, doi:10.1038/s41591-021-01377-8 (2021).
29 Stamatatos, L. *et al.* mRNA vaccination boosts cross-variant neutralizing antibodies elicited by SARS-CoV-2 infection. *Science*, doi:10.1126/science.abg9175 (2021).
30 Bergstrom, J. J., Xu, H. & Heyman, B. Epitope-Specific Suppression of IgG Responses by Passively Administered Specific IgG: Evidence of Epitope Masking. *Frontieres in Immunology* **8**, 238, doi:10.3389/fimmu.2017.00238 (2017).
31 Baum, A. *et al.* Antibody cocktail to SARS-CoV-2 spike protein prevents rapid mutational escape seen with individual antibodies. *Science* **369**, 1014-1018, doi:10.1126/science.abd0831 (2020).
32 Hansen, J. *et al.* Studies in humanized mice and convalescent humans yield a SARS-CoV-2 antibody cocktail. *Science* **369**, 1010-1014, doi:10.1126/science.abd0827 (2020).
33 Shi, R. *et al.* A human neutralizing antibody targets the receptor-binding site of SARS-CoV-2. *Nature* **584**, 120-124, doi:10.1038/s41586-020-2381-y (2020).
34 Gottlieb, R. L. *et al.* Effect of Bamlanivimab as Monotherapy or in Combination With Etesevimab on Viral Load in Patients With Mild to Moderate COVID-19: A Randomized Clinical Trial. *JAMA* **325**, 632-644, doi:10.1001/jama.2021.0202 (2021).
35 Jones, B. E. *et al.* The neutralizing antibody, LY-CoV555, protects against SARS-CoV-2 infection in nonhuman primates. *Sci Transl Med* **13**, doi:10.1126/scitranslmed.abf1906 (2021).
36 Dong, J. *et al.* Genetic and structural basis for SARS-CoV-2 variant neutralization by a two-antibody cocktail. *Nat Microbiol* **6**, 1233-1244, doi:10.1038/s41564-021-00972-2 (2021).
37 Zost, S. J. *et al.* Potently neutralizing and protective human antibodies against SARS-CoV-2. *Nature* **584**, 443-449, doi:10.1038/s41586-020-2548-6 (2020).

38 Thomson, E. C. *et al.* Circulating SARS-CoV-2 spike N439K variants maintain fitness while evading antibody-mediated immunity. *Cell* **184**, 1171-1187 e1120, doi:10.1016/j.cell.2021.01.037 (2021).
39 Starr, T. N. *et al.* ACE2 binding is an ancestral and evolvable trait of sarbecoviruses. doi:10.1101/2021.07.17.452804 (2021).
40 Lempp, F. A. *et al.* Lectins enhance SARS-CoV-2 infection and influence neutralizing antibodies. *Nature* **598**, 342-347, doi:10.1038/s41586-021-03925-1 (2021).
41 VanBlargan, L. A. *et al.* An infectious SARS-CoV-2 B.1.1.529 Omicron virus escapes neutralization by several therapeutic monoclonal antibodies. *bioRxiv*, doi:10.1101/2021.12.15.472828 (2021).
42 Aggarwa, A., Ospina Stella, A. & Walker, G. SARS-CoV-2 Omicron: evasion of potent humoral responses and resistance to clinical immunotherapeutics relative to viral variants of concern. *bioRxiv* (2021).
43 FDA. FACT SHEET FOR HEALTHCARE PROVIDERS EMERGENCY USE AUTHORIZATION (EUA) OF SOTROVIMAB. *https://www.fda.gov/media/149534/download* (2021).
44 Tortorici, M. A. *et al.* Ultrapotent human antibodies protect against SARS-CoV-2 challenge via multiple mechanisms. *Science* **370**, 950-957, doi:10.1126/science.abe3354 (2020).
45 McCallum, M. *et al.* N-terminal domain antigenic mapping reveals a site of vulnerability for SARS-CoV-2. *Cell* **184**, 2332-2347 e2316, doi:10.1016/j.cell.2021.03.028 (2021).
46 McCallum, M. *et al.* SARS-CoV-2 immune evasion by the B.1.427/B.1.429 variant of concern. *Science*, doi:10.1126/science.abi7994 (2021).
47 Fischer, W. *et al.* HIV-1 and SARS-CoV-2: Patterns in the evolution of two pandemic pathogens. *Cell Host Microbe* **29**, 1093-1110, doi:10.1016/j.chom.2021.05.012 (2021).
48 Kupferschmidt, K. Where did 'weird' Omicron come from? *Science* **374**, 1179, doi:10.1126/science.acx9738 (2021).
49 Corey, L. *et al.* SARS-CoV-2 Variants in Patients with Immunosuppression. *N Engl J Med* **385**, 562-566, doi:10.1056/NEJMsb2104756 (2021).
50 Oude Munnink, B. B. *et al.* Transmission of SARS-CoV-2 on mink farms between humans and mink and back to humans. *Science* **371**, 172-177, doi:10.1126/science.abe5901 (2021).

Additional References related to Methods

51 Zang, R. *et al.* TMPRSS2 and TMPRSS4 promote SARS-CoV-2 infection of human small intestinal enterocytes. *Sci Immunol* **5**, doi:10.1126/sciimmunol.abc3582 (2020).

52 Maziarz, R. T. *et al.* Control of an outbreak of human parainfluenza virus 3 in hematopoietic stem cell transplant recipients. *Biol Blood Marrow Transplant* **16**, 192-198, doi:10.1016/j.bbmt.2009.09.014 (2010).

53 Katoh, K. & Standley, D. M. MAFFT multiple sequence alignment software version 7: improvements in performance and usability. *Mol Biol Evol* **30**, 772-780, doi:10.1093/molbev/mst010 (2013).

54 Yamin, R. *et al.* Fc-engineered antibody therapeutics with improved anti-SARS-CoV-2 efficacy. *Nature* **599**, 465-470, doi:10.1038/s41586-021-04017-w (2021).

55 Giroglou, T. *et al.* Retroviral vectors pseudotyped with severe acute respiratory syndrome coronavirus S protein. *J Virol* **78**, 9007-9015, doi:10.1128/JVI.78.17.9007-9015.2004 (2004).

56 Walls, A. C. *et al.* Elicitation of broadly protective sarbecovirus immunity by receptor-binding domain nanoparticle vaccines. *Cell* **184**, 5432-5447 e5416, doi:10.1016/j.cell.2021.09.015 (2021).

57 Kaname, Y. *et al.* Acquisition of complement resistance through incorporation of CD55/decay-accelerating factor into viral particles bearing baculovirus GP64. *J Virol* **84**, 3210-3219, doi:10.1128/JVI.02519-09 (2010).

58 Plante, J. A. *et al.* Spike mutation D614G alters SARS-CoV-2 fitness. *Nature*, doi:10.1038/s41586-020-2895-3 (2020).

59 Imai, M. *et al.* Syrian hamsters as a small animal model for SARS-CoV-2 infection and countermeasure development. *Proc Natl Acad Sci U S A* **117**, 16587-16595, doi:10.1073/pnas.2009799117 (2020).

60 Liu, Z. *et al.* Identification of SARS-CoV-2 spike mutations that attenuate monoclonal and serum antibody neutralization. *Cell Host Microbe* **29**, 477-488.e474, doi:10.1016/j.chom.2021.01.014 (2021).

61 VanBlargan, L. A. *et al.* A potently neutralizing SARS-CoV-2 antibody inhibits variants of concern by utilizing unique binding residues in a highly conserved epitope. *Immunity*, doi:10.1016/j.immuni.2021.08.016 (2021).

62 Cathcart, A. L. *et al.* The dual function monoclonal antibodies VIR-7831 and VIR-7832 demonstrate potent in vitro and in vivo activity against SARS-CoV-2. *bioRxiv*, 2021.2003.2009.434607, doi:10.1101/2021.03.09.434607 (2021).

63 Gupta, A. *et al.* Early Treatment for Covid-19 with SARS-CoV-2 Neutralizing Antibody Sotrovimab. *N Engl J Med* **385**, 1941-1950, doi:10.1056/NEJMoa2107934 (2021).

64 Kim, C. *et al.* A therapeutic neutralizing antibody targeting receptor binding domain of SARS-CoV-2 spike protein. *Nat Commun* **12**, 288, doi:10.1038/s41467-020-20602-5 (2021).

65 Ryu, D. K. *et al.* Therapeutic effect of CT-P59 against SARS-CoV-2 South African variant. *Biochem Biophys Res Commun* **566**, 135-140, doi:10.1016/j.bbrc.2021.06.016 (2021).

66 Baum, A. *et al.* REGN-COV2 antibodies prevent and treat SARS-CoV-2 infection in rhesus macaques and hamsters. *Science* **370**, 1110-1115, doi:10.1126/science.abe2402 (2020).

67 Copin, R. *et al.* The monoclonal antibody combination REGEN-COV protects against SARS-CoV-2 mutational escape in preclinical and human studies. *Cell* **184**, 3949-3961 e3911, doi:10.1016/j.cell.2021.06.002 (2021).
68 Weinreich, D. M. *et al.* REGN-COV2, a Neutralizing Antibody Cocktail, in Outpatients with Covid-19. *N Engl J Med* **384**, 238-251, doi:10.1056/NEJMoa2035002 (2021).
69 Chen, P. *et al.* SARS-CoV-2 Neutralizing Antibody LY-CoV555 in Outpatients with Covid-19. *N Engl J Med* **384**, 229-237, doi:10.1056/NEJMoa2029849 (2021).
70 Group, A.-T. L.-C. S. *et al.* A Neutralizing Monoclonal Antibody for Hospitalized Patients with Covid-19. *N Engl J Med* **384**, 905-914, doi:10.1056/NEJMoa2033130 (2021).
71 Belk, J., Deveau, L. M., Rappazzo, C. G., Walker, L. & Wec, A. WO2021207597 - COMPOUNDS SPECIFIC TO CORONAVIRUS S PROTEIN AND USES THEREOF. *ADAGIO THERAPEUTICS, INC.* (2021).

nature portfolio

Corresponding author(s): Davide Corti, David Veesler

Last updated by author(s): Dec 21, 2021

Reporting Summary

Nature Portfolio wishes to improve the reproducibility of the work that we publish. This form provides structure for consistency and transparency in reporting. For further information on Nature Portfolio policies, see our Editorial Policies and the Editorial Policy Checklist.

Statistics

For all statistical analyses, confirm that the following items are present in the figure legend, table legend, main text, or Methods section.

n/a	Confirmed	
☐	☒	The exact sample size (*n*) for each experimental group/condition, given as a discrete number and unit of measurement
☐	☒	A statement on whether measurements were taken from distinct samples or whether the same sample was measured repeatedly
☐	☒	The statistical test(s) used AND whether they are one- or two-sided *Only common tests should be described solely by name; describe more complex techniques in the Methods section.*
☒	☐	A description of all covariates tested
☒	☐	A description of any assumptions or corrections, such as tests of normality and adjustment for multiple comparisons
☐	☒	A full description of the statistical parameters including central tendency (e.g. means) or other basic estimates (e.g. regression coefficient) AND variation (e.g. standard deviation) or associated estimates of uncertainty (e.g. confidence intervals)
☐	☒	For null hypothesis testing, the test statistic (e.g. *F*, *t*, *r*) with confidence intervals, effect sizes, degrees of freedom and *P* value noted *Give P values as exact values whenever suitable.*
☒	☐	For Bayesian analysis, information on the choice of priors and Markov chain Monte Carlo settings
☒	☐	For hierarchical and complex designs, identification of the appropriate level for tests and full reporting of outcomes
☒	☐	Estimates of effect sizes (e.g. Cohen's *d*, Pearson's *r*), indicating how they were calculated

Our web collection on statistics for biologists contains articles on many of the points above.

Software and code

Policy information about availability of computer code

Data collection	Sequences and metadata were obtained from GISAID (https://www.epicov.org/). Both metadata and fasta files of all sequences annotated with the BA.1 lineage were downloaded on 20DEC2021 at 8.30pm PST. SPR binding data were collected using Biacore T200 Control Software, v. 2.0.2
Data analysis	As detailed in the materials and methods, "collection date" and "country" fields were extracted from the metadata file. Spike protein sequences were extracted from the genome fasta files and aligned to the Wuhan-1 reference spike protein. The prevalence of mutations present in the BA.1 lineage was extracted in R (4.0.2, https://www.R-project.org/), considering only un-ambiguous residues in both nominator and denominator. Sequence counts per country and/or per week were extracted in R and plotted with ggplot2 3.3.2 (https://ggplot2.tidyverse.org) and sf 0.9-7 (https://doi.org/10.32614/RJ-2018-009) packages. BioPharma Finder 3.2 and GPMAW 285 10.10 software were used for analysis by LC/MS of intact protein mass. Neutralization assays were analyzed using GraphPad Prism (Version 9.1.0) as described in Methods. Biacore T200 Evaluation Software, v. 3.1, was used to fit models to the ACE2 binding data.

For manuscripts utilizing custom algorithms or software that are central to the research but not yet described in published literature, software must be made available to editors and reviewers. We strongly encourage code deposition in a community repository (e.g. GitHub). See the Nature Portfolio guidelines for submitting code & software for further information.

Data

Policy information about availability of data

All manuscripts must include a data availability statement. This statement should provide the following information, where applicable:

- Accession codes, unique identifiers, or web links for publicly available datasets
- A description of any restrictions on data availability
- For clinical datasets or third party data, please ensure that the statement adheres to our policy

Materials generated in this study will be made available on request and may require a material transfer agreement. GISAID (www.gisaid.org) data access requires registration. Note: after consulting with the local Ethical authority, due to health and data protection laws relating to the demographic and clinical information contained in the manuscript, we will not be able to fully comply with the requirement to share demographic and clinical data of individual patients/ donors in this study.

Field-specific reporting

Please select the one below that is the best fit for your research. If you are not sure, read the appropriate sections before making your selection.

☒ Life sciences ☐ Behavioural & social sciences ☐ Ecological, evolutionary & environmental sciences

For a reference copy of the document with all sections, see nature.com/documents/nr-reporting-summary-flat.pdf

Life sciences study design

All studies must disclose on these points even when the disclosure is negative.

Sample size	N/A. Sample size for samples from covalescent/vaccinated individuals was chosen according to or exceeding standards in the field, and in most cases exceeded 10 samples per group.
Data exclusions	monoclonal antibodies that did not show a reliable neutralization curve with SARS-CoV-2 Wuhan S VSV pseudotypes were excluded from the analysis.
Replication	Experimental assays were performed at least in two independent replicates. Each replicate was performed with 2, 3, or more technical repeats or was done in biological triplicate according to or exceeding standards in the field. We conducted all neutralization and antibody functional assays in biological duplicate, triplicate, or more, as indicated in relevant figure legends. In all cases, representative figure displays were appropriately indicated.
Randomization	Randomization was not a relevant feature as we were applying a uniform set of techniques across a panel of sera/plasma or monoclonal antibodies.
Blinding	Blinding was not a relevant feature as we were applying a uniform set of techniques across a panel of sera/plasma or monoclonal antibodies and tests were repeated two or more times by different individuals.

Reporting for specific materials, systems and methods

We require information from authors about some types of materials, experimental systems and methods used in many studies. Here, indicate whether each material, system or method listed is relevant to your study. If you are not sure if a list item applies to your research, read the appropriate section before selecting a response.

Materials & experimental systems

n/a	Involved in the study
☐	☒ Antibodies
☐	☒ Eukaryotic cell lines
☒	☐ Palaeontology and archaeology
☒	☐ Animals and other organisms
☐	☒ Human research participants
☒	☐ Clinical data
☒	☐ Dual use research of concern

Methods

n/a	Involved in the study
☒	☐ ChIP-seq
☒	☐ Flow cytometry
☒	☐ MRI-based neuroimaging

Antibodies

Antibodies used	Sotrovimab and NTD- and RBD-specific antibodies discovered at VIR Biotechnology were produced as recombinant IgG1 in mammalian cells as described in material and methods, see details in Extended Data Table 2. As to the other therapeutic mAbs were cloned and produced according to publicly available sequences: VH and VL sequences for mAbs COV2-2130 (PDB ID 7L7E),

	COV2-2196 (PDB ID 7L7E, 7L7D), REGN10933 (PDB ID 6XDG), REGN10987 (PDB ID 6XDG) and ADI-58125 (PCT application WO2021207597, seq. IDs 22301 and 22311), LY-CoV555 (PDB ID 7KMG), LY-CoV016 (PDB ID 7C01), and CT-P59 (PDB ID 7CM4) All the commercial antibodies used in the study have been indicted with supplier name, catalog number.
Validation	The identity of the produced monoclonal antibodies (produced recombinantly as human IgG1) was confirmed by LC-MS analysis.

Eukaryotic cell lines

Policy information about cell lines

Cell line source(s)	Cell lines used in this study were obtained from ATCC (HEK293T and Vero E6), ThermoFisher Scientific (Expi CHO cells, FreeStyle™ 293-F cells and Expi293F™ cells) Lenti-X 293T cells (Takara) or generated in-house (Vero E6/TMPRSS2)
Authentication	None of the cell lines used were authenticated
Mycoplasma contamination	Cell lines were not tested for mycoplasma contamination
Commonly misidentified lines (See ICLAC register)	No commonly misidentified cell lines were used in the study

Human research participants

Policy information about studies involving human research participants

Population characteristics	Samples were collected 14-28 days after symptoms onset and 14-28 days after vaccination (with the exception of individuals vaccinated with Ad26.COV2.S where samples were collected 1-19 weeks affter 1st vaccine dose). Details on patients demographics is provided in Extended Data Table 1
Recruitment	Patients were recruited on the basis of prior SARS-CoV-2 infection or vaccination in the hospital or outpatient setting. Patients were healthy volunteers who donated blood after being informed about the study. The only exclusion criteria used were HIV or other debilitating disease, but other information about diagnosis and treatment was not collected. Convalescent plasma, Ad26.COV2.S, mRNA-1273 and BNT162b2 samples were obtained from the HAARVI study approved by the University of Washington Human Subjects Division Institutional Review Board (STUDY00000959). AZD1222 samples were obtained from INGM, Ospedale Maggio Policlinico of Milan and approved by the local review board Study Polimmune. Sputnik V samples were obtained from healthcare workers at the hospital de Clínicas "José de San Martín", Buenos Aires, Argentina. Sinopharm vaccinated individuals were enrolled from Aga Khan University under IRB of UWARN study.
Ethics oversight	Study protocols for antibody isolation were approved by the local Institutional Review Board (Canton Ticino Ethics Committee, Switzerland), and all donors provided written informed consent for the use of blood and blood components. Study protocols for serological assays were approved by the local Institutional Review Boards relevant for each of three cohorts of samples (Canton Ticino Ethics Committee, Switzerland, the Ethical Committee of Luigi Sacco Hospital, Milan, Italy, and University of Washington Human Subjects Division Institutional Review Board. All donors provided written informed consent for the use of blood and blood components (such as PBMCs, sera or plasma) and were recruited at hospitals or as outpatients.

Note that full information on the approval of the study protocol must also be provided in the manuscript.